Convective Turbulence

1 Rayleigh-Taylor Convection

Convection is a gravitational instability that occurs when denser fluid overlies lighter fluid, and the associated vertical acceleration overcomes the molecular diffusion of buoyancy and induces motion. An initial value representation of this is known as Rayleigh-Taylor convection. The simplest configuration of this problem consists of a two-layer system such that

$$\rho = \begin{cases} \rho_0 + \delta\rho & H/2 < z < H \\ \rho_0 - \delta\rho & 0 < z < H/2 \end{cases} \quad \text{where } \delta\rho > 0, \tag{1}$$

and the gravitational acceleration $\mathbf{g} = -g\widehat{z}$. While this a configuration can satisfy hydrostatic balance, infinitesimal perturbations on the interface separating the two fluids at $z = H/2$ will grow exponentially, leading to overturning. The energy available for overturning can be estimated by considering the fluid energetics. The average potential energy (per unit volume) of the system described by (1) is

$$P = \frac{1}{H} \int_0^H \rho gz\, dz = \rho_0 gH \left[\frac{1}{2} + \left(\frac{\delta\rho}{\rho_0} \right) \frac{1}{4} \right] . \tag{2}$$

Therefore, a simple overturning of the fluid to reverse the sign of the density jump from positive upward to negative reduces the potential energy of the system by the amount

$$\Delta P = \frac{gH\delta\rho}{2} . \tag{3}$$

In principal ΔP can be used to do work, most simply by transformation into kinetic energy; in simplest terms the transformation might induce a vertical *free-fall velocity* w_f whose kinetic energy $\rho_0 w_f^2/2$ is equal to ΔP. In practice, however, the fluid cannot overturn without some mixing induced by the motion (through a turbulent cascade if Re is large enough). Mixing increases the entropy of the system and bounds the amount of work that ΔP can do. Paradoxically, the more the diffusivity of the fluid is reduced, the more turbulent the fluid becomes, and the more effectively it mixes.

Bounds on the energy that can be extracted from the unstable configuration of the flow can be determined by considering the entropy, s. From the first and second laws, for a single-component fluid,

$$T ds = dh - \alpha dp \tag{4}$$

where $h = c_p T$ is the enthalpy and α is the specific volume. Neglecting changes in the pressure from that of the isothermal reference state, this implies that

$$s = s_0 + c_p \ln(T/T_0) . \tag{5}$$

s_0 denotes the reference state entropy, corresponding to the reference state temperature T_0. The average entropy per unit volume of the system is

$$S = \frac{1}{H} \int_0^H \rho s\, dz = \frac{1}{H} \int_0^H \rho\left(s_0 + c_p \ln(T/T_0) \right) dz . \tag{6}$$

For (1), in the limit of small temperature/density, so that the Boussinesq approximation is valid (*i.e.,* $\delta\rho/\rho_0 = -\delta T/T_0$ with both small quantities)),

$$S = S_0 - \frac{3\rho_0 c_p}{2} \left(\frac{\delta T}{T_0}\right)^2 \leq S_0 . \tag{7}$$

The system entropy depends only on the temperature differences, not on their sign, and maximizes for a well mixed fluid, *i.e.,* one in which $\delta T = 0$. Thus the system is stable only when well mixed in T (or unstratified) since this corresponds to a state of maximum entropy. From (2) the release of potential energy that would occur in a transition to a well mixed state is $\Delta P/2$; this bounds the amount of work the overturning can do. In the limit of high Reynolds (and Peclet) numbers we might expect the development of a wide range of scales with an energy spectral density $E(k)$ peaking near the overturning length scale $H/2$ and bounded such that

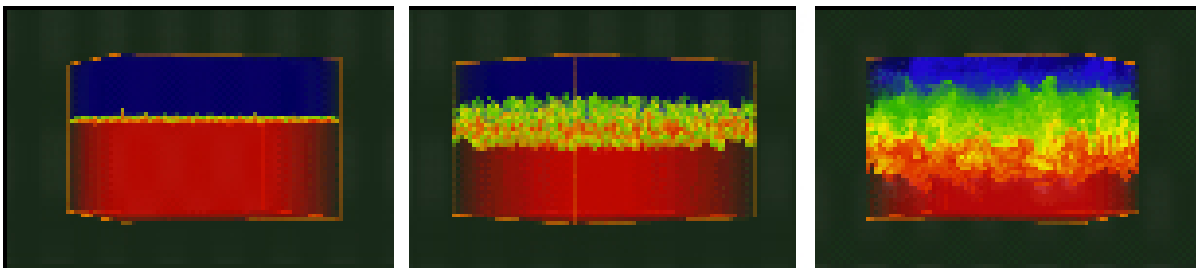$$\int E(k)\,\mathrm{d}k \leq \frac{\Delta P}{2} . \tag{8}$$

Figure 1: Temperature visualization in a simulation of temporally developing Rayleigh-Taylor instability. (From `http://www.llnl.gov/casc/asciturb/simulations.shtml`)

The problem of Rayleigh-Taylor instability is a generic paradigm for convection. It provides an interesting test problem for numerical simulation, where we can ask how the energy spectrum develops and decays as a function of resolution and numerical technique. An example of visualizations from such computation are shown in Fig. 1-2.

The Rayleigh-Taylor problem is also a useful paradigm for continuously stratified fluids, whereby the negative entropy gradient, $ds/dz < 0$ measures the potential for convective overturning. For dry air $s = \ln\theta$ where θ is the potential temperature. For saturated air with constant specific humidity, $s = c_p \ln\theta_e$ where θ_e is the equivalent potential temperature. Moist, but unsaturated systems with decreasing θ_e but increasing θ are said to be potentially unstable as they become gravitationally unstable (*i.e.,* convective) only when parcels are brought to saturation, for instance through the expansionary cooling that can happen when a moist layer is lifted through the atmosphere.
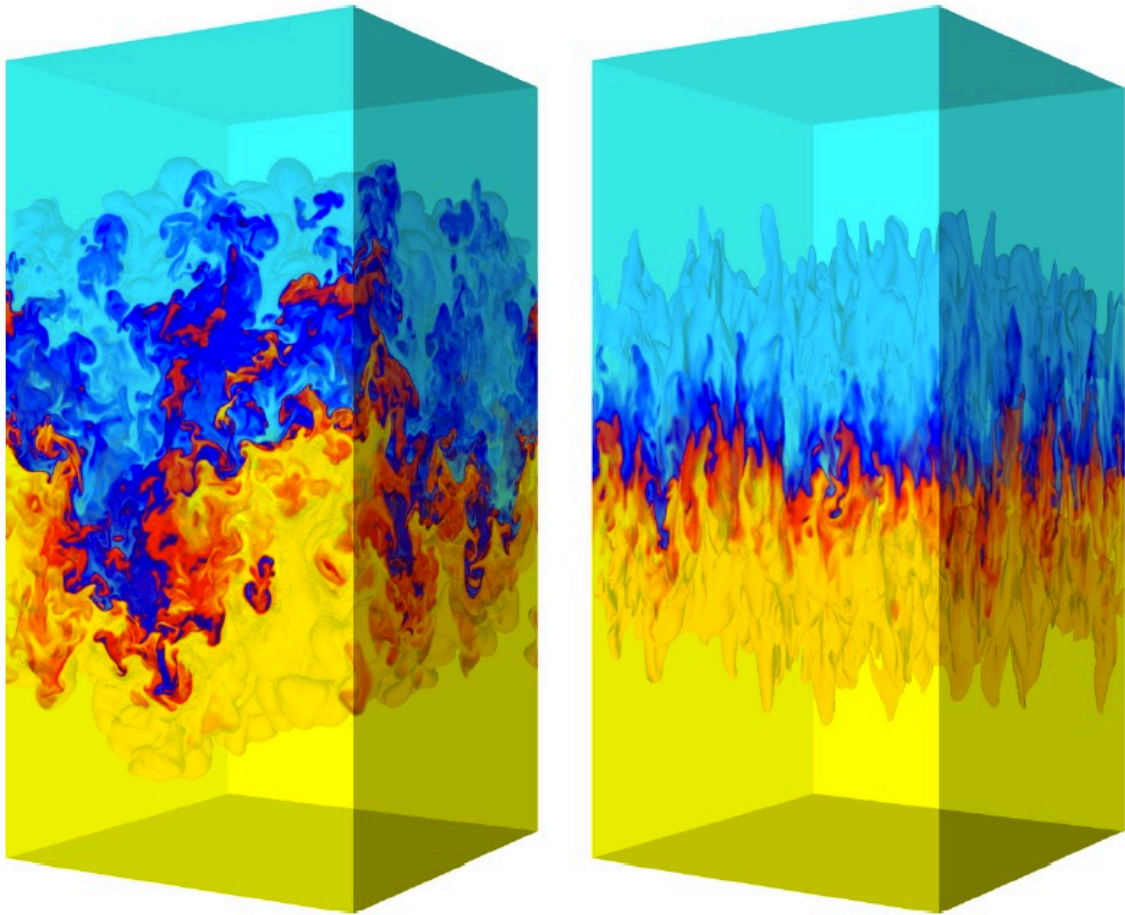
Figure 2: Temperature visualizations in a simulation of temporally developing Rayleigh-Taylor instability (left) without and (right) with rotation. Yellow (blue) represents hot (cold), light (heavy) fluid. (Boffetta *et al.*, 2016)
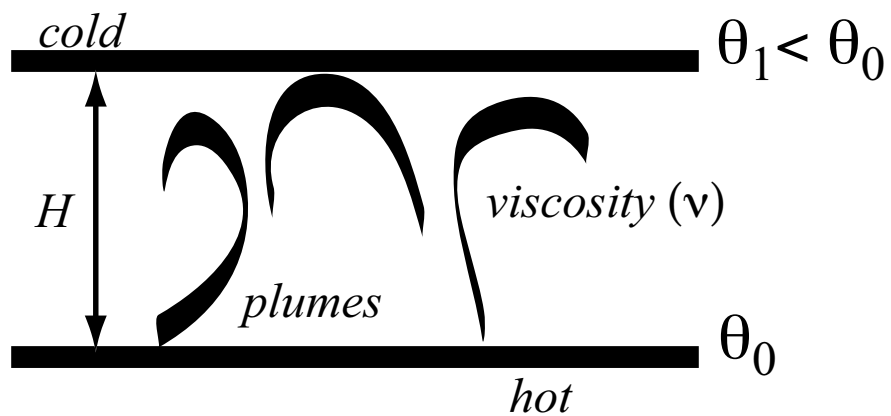

Figure 3: Basic configuration for the Rayleigh-Benard convective instability problem.

2 Rayleigh-Benard Convection

Another basic paradigm of convection is Rayleigh-Benard convection [1]. This type of convection is the type a Boussinesq fluid would experience in layer heated from below and cooled from above in a vertically bounded domain; this experimental situation is illustrated schematically in Fig. 3. If Rayleigh-Taylor is the initial value paradigm for convective turbulence — the transient adjustment of a convectively unstable fluid — then Rayleigh-Benard convection is the boundary value paradigm — the structure of the turbulence for a continually destabilized fluid with top and bottom boundary layers. In Rayleigh Benard convection we are interested in the structure of a turbulent layer forced by a constant buoyancy flux, for instance in a fluid mediating the heat transfer between an upper cold and a lower hot reservoir.

Many questions can be asked regarding the structure of the flow regime that arises in such a situation, but perhaps the first and foremost is under what conditions will the flow become unstable? This question fits within the general sequence of transition regimes discussed in *Turbulent Flows*. Unlike in the Rayleigh-Taylor discussion, molecular effects are explicitly accounted for in the Rayleigh-Bérnard problem, and the first instability for a mean state of motionless, conductive buoyancy flux occurs at a finite value of Ra in (9). The diffusive transport of heat tends to counter the gravitationally destabilizing influence of the heating until the heating rate becomes strong enough (*i.e.,* Ra large enough) for a linear instability to occur (Appendix).

Whereas ΔP describes how strongly forced the convective overturning is in the Rayleigh-Taylor problem; the Rayleigh number,

$$Ra = \frac{BH^3}{\nu\kappa}, \tag{9}$$

measures how strongly the convection is being driven in the Rayleigh-Benard problem. Ra can also be thought of as a non-dimensional measure of the importance of nonlinearity in the transport of buoyancy within the fluid, somewhat analogous to the Reynolds number; more precisely, $Ra \sim Re^2$ when the velocity magnitude in Re is determined from free-fall acceleration of a gravitationally unstable buoyancy profile (see the *Turbulent Flows* notes). H is the convective layer depth, and $B > 0$ is a characteristic unstable buoyancy difference; *e.g.,* $B = -\alpha g \Delta T$ if the source of the buoyancy difference is a negative temperature difference $\Delta T < 0$ (where α is the coefficient of thermal expansion). When Ra is small enough, the buoyancy transport is conductive with no fluid motion required. For $Ra \approx 10^3$, convection arises. At the first bifurcation from a state of rest, the spatial pattern of convective motions is parallel roll cells, a 2D pattern, but there are further bifurcations to more complex patterns (*e.g.,* , hexagonal cells, as in Fig. 4). At large enough Ra, the pattern of convection loses its global order (*i.e.,* spatial periodicity), and fully developed convection ensues. The coherent structures of this latter regime are called *buoyant plumes*, and typically they have no large-scale order among themselves.

Here we will restrict our consideration to the simply configured Rayleigh-Benard problem that is nearly homogeneous, but not entirely so because of the vertical boundaries. This problem has a well defined equilibrium state for steady boundary conditions, and it is easily realized both in the laboratory and in simulations. Consider a layer of depth H between two solid plates, with either

---

[1]Rayleigh developed his theory as an attempt to explain the observations of Benard. It is ironic that some of these observations later were shown to be due more to variations in the surface tension with temperature than to thermal instability.
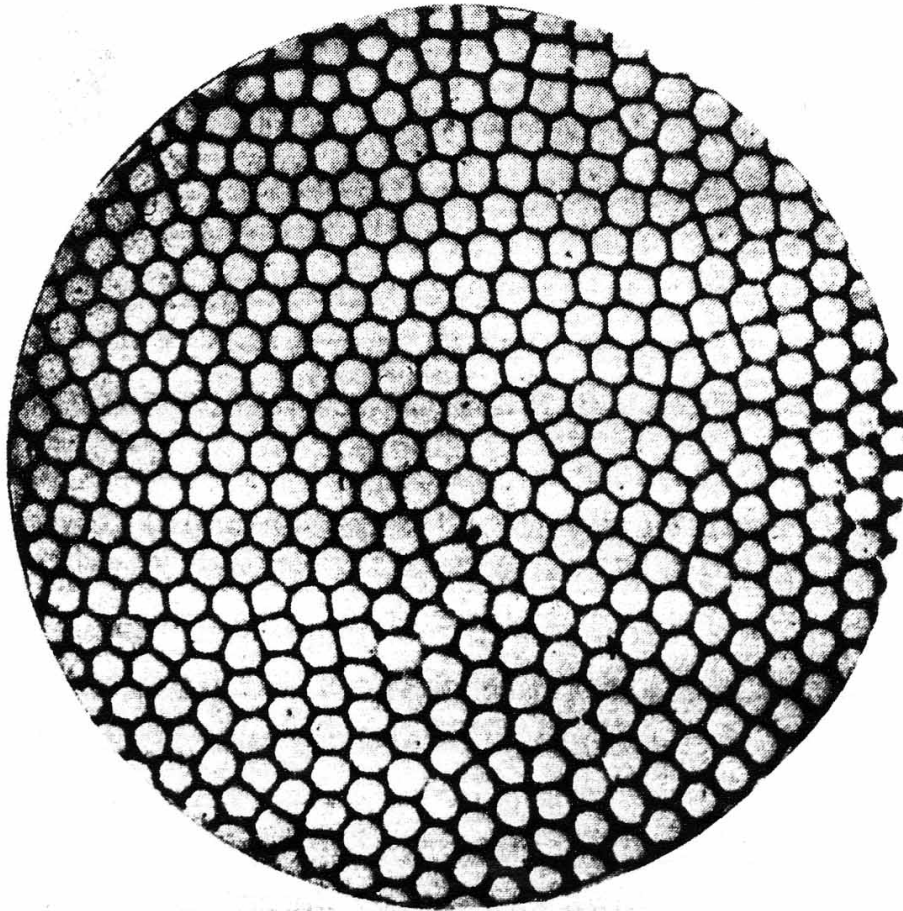
Figure 4: Convection cells in spermaceti at a modestly supercritical Ra value. This a reproduction of one of Benard's original photographs *via* Chandrasekhar (1961).
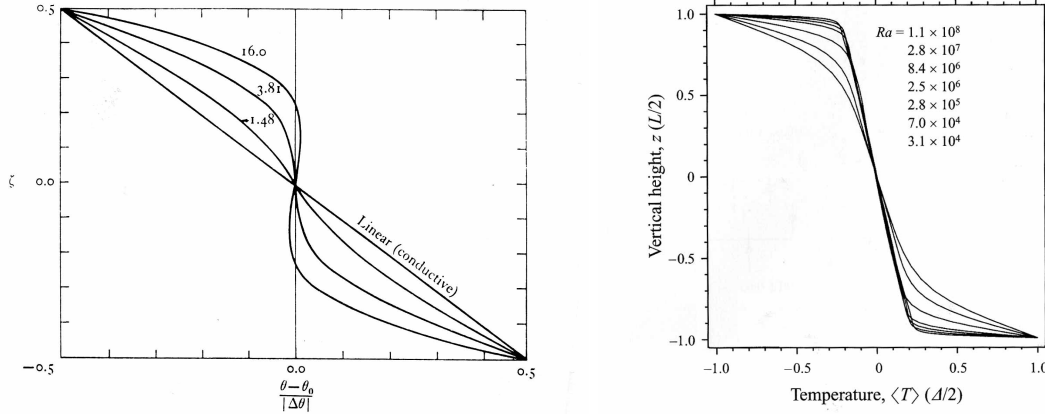
Figure 5: Vertical profiles of mean temperature in Rayleigh-Benard convection. (Left) Non-rotating convection, for several different values of $\lambda = Ra/Ra_c$ (Turner, 1973). (Right) Rotating convection for several different values of Ra with fixed $Ro = \sqrt{Ra/PrTa} = 0.75$ (Julien *et al.*, 1996). Note that for large Ra non-rotating convection attains a weakly stable interior profile while rotating convection remains persistently unstable.

uniform but unequal values of b on the plates (*i.e.,* $\overline{b}(H/2) - \overline{b}(-H/2) \equiv -B$) or uniform and equal positive buoyancy fluxes through the plates, $\mathcal{B} > 0$. In the resulting convective phenomena, this difference of buoyancy boundary conditions is not very important.[2] As Ra increases — as the fluid state moves through conduction, globally ordered cellular patterns, and locally ordered plumes — the mean buoyancy profile $\overline{b}(z)$, changes from the vertically uniform gradient of the conductive state to a non-uniform state where most of the gradient occurs in *buoyancy boundary layers* near $z = \pm H/2$, and the interior gradient gets increasingly small and may even reverse in sign (*i.e.,* become locally gravitationally stable) for some values of the Prandtl number $Pr = \nu/\kappa$ (Fig. 5, left panel, for air, with $Pr = 7$). The usual explanation for the weak or stable interior gradient found at at large Ra is that a plume, which is formed within one boundary layer, is very effective in retaining its anomalously buoyant core material while crossing the interior region, surrendering it up to more general mixing only after reaching the opposite boundary layer. As we will see, there is some mixing *en route* between a plume and its environment, often called entrainment, but many plumes retain their integrity entirely across the convecting layer, especially in the presence of internal heating (*e.g.,* from cumulus condensation). In rotating convection,

---

[2]There is a long history of alternatively posing the Rayleigh-Benard problem either in terms of the buoyancy difference B or in terms of the buoyancy flux $\mathcal{B}$. In the two situations, there are analogous non-dimensional Ra and Ro numbers and the free-fall velocity (defined elsewhere in the chapter); *viz.,*

$$Ra = \frac{BH^3}{\nu\kappa} \quad \text{or} \quad Ra = \frac{\mathcal{B}^{2/3}H^{8/3}}{\nu\kappa} \, ,$$

$$Ro = \frac{B^{1/2}}{fH^{1/2}} \quad \text{or} \quad Ro = \frac{\mathcal{B}^{1/3}}{fH^{2/3}} \, ,$$

$$w_f = (BH)^{1/2} \quad \text{or} \quad w_f = (\mathcal{B}H)^{1/3} \, .$$

however, plume entrainment is much more efficient since the plumes are also cyclonic vortices, and the interior mean buoyancy gradient equilibrates at a finite negative value (Sec. 4).

At the boundary, where the velocity vanishes due to the kinematic condition of no normal flow and the viscous condition of no tangential slip, the buoyancy flux must be entirely conductive, in particular in the vertical direction,

$$-\kappa \frac{\partial \overline{b}}{\partial z} = \mathcal{B} \tag{10}$$

at $z = \pm H/2$. As Ra increases, either because κ decreases or $|\mathcal{B}|$ increases, then $\left| \partial_z \overline{b}(\pm H/2) \right|$ must also increase. Since the vertical buoyancy flux must be equal to $\mathcal{B}$ at all z throughout the layer in equilibrium,

$$\mathcal{B} = \overline{w'b'} - \kappa \frac{\partial \overline{b}}{\partial z} = const. \, . \tag{11}$$

The turbulent flux must dominate in the interior where $\partial_z \overline{b}$ is small, whether negative or even positive. Thus, if we attempt an eddy-diffusion interpretation in the interior,

$$\kappa_e(z) = -\mathcal{B} \Big/ \frac{\partial \overline{b}}{\partial z}(z) \, , \tag{12}$$

the value of κ_e will be very large and maybe even negative. If the value is large, then clearly $\kappa_e(z)$ is spatially quite non-uniform (*cf.,* fully developed turbulence in Couette shear flow). If κ_e is negative, this has very disconcerting implications (*i.e.,* unmixing behavior for fluctuations), and therefore it should be rejected as a meaningful diagnostic language for interpreting the effects of the turbulence. The fallacy, of course, arises from making a local interpretation of an essentially non-local process, the passage of coherent, fluid-retaining plumes across the interior of the domain. We would have had to make a similar rejection for the free shear layer or shear boundary layer if the resulting $K_e(z)$ were not so simple in its structure and everywhere positive, but evidently the associated turbulent momentum transport by hairpin vortices in shear is leakier than is the plume buoyancy flux in convection.

We define the *Nusselt number*, Nu as the ratio of the mean buoyancy flux to its value in the conducting state,

$$Nu = \frac{|\mathcal{B}|H}{\kappa B} \geq 1 \, . \tag{13}$$

Obviously, we expect Nu to be an increasing function of Ra, as the turbulent component of the transport becomes ever more dominant. What is of particular interest is the possibility of self-similar, or *scaling*, behavior, defined as a power-law dependence in the Nusselt number, $Nu \propto Ra^\gamma$ for some $\gamma > 0$. This can be interpreted as an essential similarity of the turbulent dynamics throughout such a scaling regime, with only quantitative changes in the statistics with increasing Ra or Re. Interestingly it turns out that there seem to be at least two such scaling regimes for fully developed Rayleigh-Benard convection.

Figure 6 shows $Nu(Ra)$ through the transition regime with modest Ra values, where particular bifurcations are evident as changes in the slope of this function. In the fully developed regime (Fig. 7), however, we see two regimes of power-law dependence (*i.e.,* scaling behavior), which have come to be called *soft* and *hard turbulence*, respectively (Siggia, 1994). In the lower-Ra, soft-turbulence regime, the dependence is

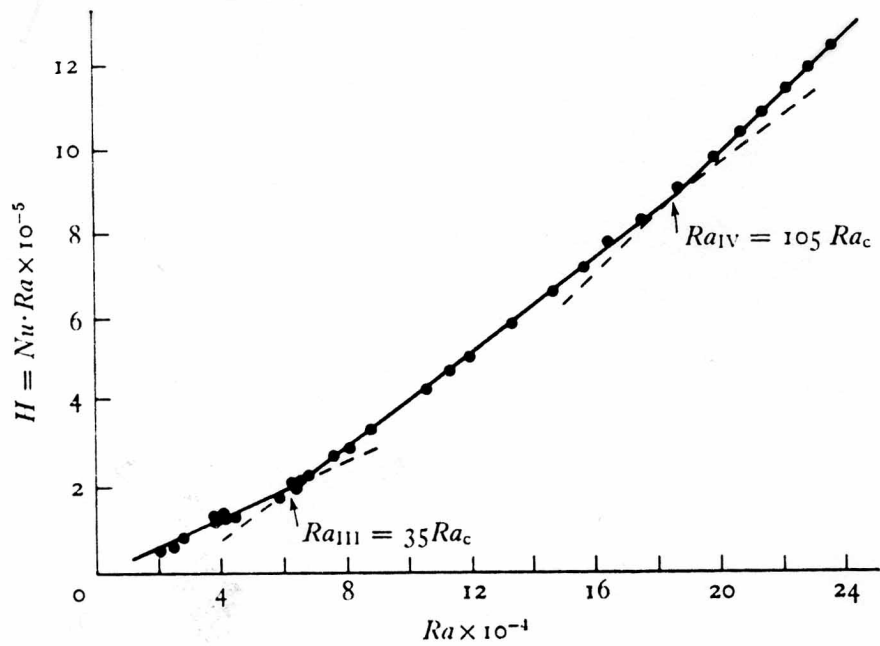$$Nu \sim Ra^{1/3} \, . \tag{14}$$

7

Figure 6: The $Nu - Ra$ correlation at intermediate Ra values, displayed here as the mean vertical heat flux, $H = NuRa$ vs. Ra. Note the occurrence of the so-called III and IV transitions at 35 Ra_c and 105 Ra_c, respectively. (From Turner, 1973)
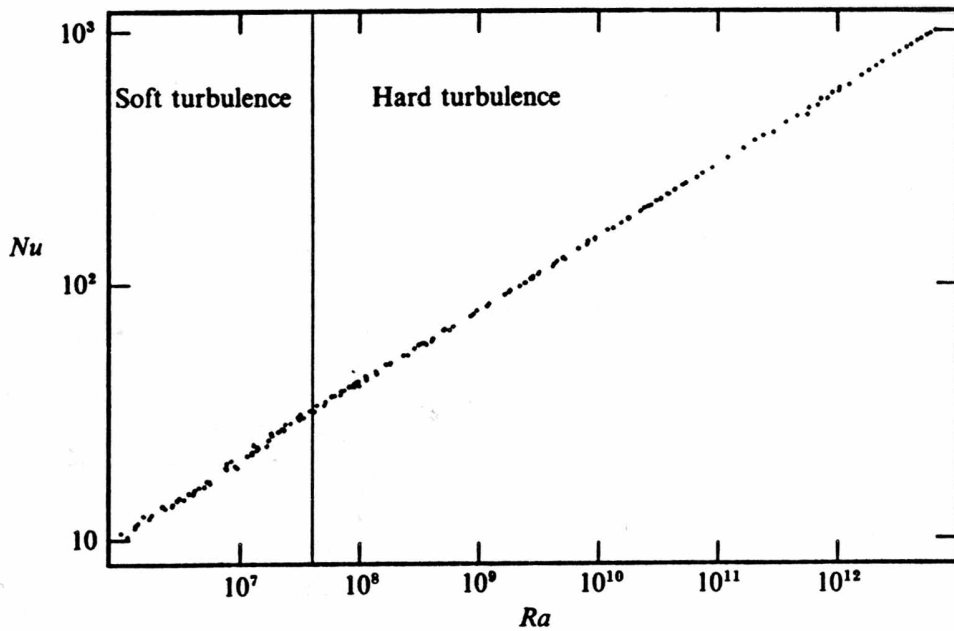

Figure 7: The $Nu - Ra$ correlation at large Ra values. The vertical line at $Ra = 4 \times 10^7$ indicates the transition from soft to hard turbulence. (Castaing *et al.*, 1989)

A theoretical interpretation for this (Malkus, 1954) is that the buoyancy flux is controlled entirely by the boundary layer processes, not the interior, so that $\mathcal{B}$ must be independent of the size of the domain, H, hence Nu in (13) must vary linearly with H; the exponent $1/3$ satisfies this condition. Equivalently, one can say that a local Rayleigh number, $Ra_b = B\delta_b^3/\nu\kappa = Ra\,(\delta_b/H)^3$ based on the boundary-layer thickness δ_b, is pegged at a marginally critical value $Ra_{cr} = \mathcal{O}(10^3)$. This implies a scaling dependence of

$$\frac{\delta_b}{H} \sim Ra^{-1/3}. \tag{15}$$

This can also be expressed as saying the buoyancy flux is comparable to the diffusive part across the buoyancy boundary layer,

$$\mathcal{B} \sim \kappa \frac{B}{\delta_b} \quad \Rightarrow \quad \frac{\delta_b}{H} \sim Nu^{-1}, \tag{16}$$

using the Nu definition (13).

In the higher-Ra, hard-turbulence regime, however, the measured Nu dependence is approximately

$$Nu \sim Ra^{2/7}, \tag{17}$$

and δ_b varies as $Ra^{-2/7}$. Several theoretical interpretations have been offered for (17). The one that seems to me most consistent with its occurrence, also in rotating convection (Sec. 4), is by Shraiman and Siggia (1990). It is based essentially on two assumptions. The first assumption is that the overall energetic balance for the flow, with mean kinetic energy dissipation equal to potential energy generation from the buoyancy flux,

$$\varepsilon = \mathcal{B}, \tag{18}$$

has the primary kinetic energy dissipation occur at a rate set by the wall stress due to the large eddies of the convection, but the dissipation itself is distributed throughout the entire convective layer, *i.e.,*

$$\varepsilon \sim H^{-1}u_*^3. \tag{19}$$

(The meaning of $\sim$ here is essentially that of dimensional analysis, and all proportionality constants are ignored in such scaling relations, in practice being written as if their value were unity.) With the definitions of Ra and Nu in (9) and (13) above, this energy balance and dissipation scaling imply

$$\begin{aligned} Ra\,Nu &\sim \frac{H^3}{\nu\kappa^2}u_*^3 \\ &\sim Re_*^3 Pr^2, \end{aligned} \tag{20}$$

where

$$Re_* \equiv \frac{u_* H}{\nu}. \tag{21}$$

The second assumption is that the momentum boundary-layer depth, δ_u, is larger than the buoyancy boundary-layer depth, δ_b, as $Ra \to \infty$. In this case, the horizontal velocity will have its viscous

9

sub-layer form, $u \sim u_*^2 z/\nu$, and the local buoyancy balance will be

$$u\, \partial_x b \approx \kappa \partial_{zz} b$$
$$\frac{u_*^2 z}{\nu\kappa} \partial_x b \approx \partial_{zz} b \,. \tag{22}$$

This has a similarity solution form

$$b \sim B\mathcal{F}\left[\frac{z}{(x\nu\kappa/u_*^2)^{1/3}}\right] \,, \tag{23}$$

for some non-dimensional profile functional $\mathcal{F}$ where $\mathcal{F} \to 0$ when its argument gets large, indicating that the magnitude of buoyancy change B across the boundary layer is of the same size as the drop across the domain as a whole (*n.b.,* Fig. 5). Thus, large-eddy flows with unit aspect ratio (*i.e.,* $x \sim H$) will have a buoyancy boundary layer thickness,

$$\delta_b \sim \left(\frac{H\nu\kappa}{u_*^2}\right)^{1/3} \quad \Rightarrow \quad \frac{\delta_b}{H} \sim Re_*^{-2/3} Pr^{-1/3} \,, \tag{24}$$

which results from a dominant balance in the buoyancy equation as indicated just above. Combining (16), (20), and (24), we obtain the scaling dependencies,

$$Nu \sim Pr^{-1/7} Ra^{2/7}, \quad Re_* \sim Pr^{-5/7} Ra^{3/7} \,, \tag{25}$$

which are consistent with the measurements in the hard-turbulence regime (Fig. 7), though not equivalent to the simple free-fall argument above that gives $Re \sim Ra^{1/2}$.

We can estimate the momentum boundary layer thickness δ_u with a horizontal momentum balance analogous to the buoyancy balance above, $u\partial_x u \approx \nu\partial_{zz} u$, applied in a bulk sense over the layer as a whole, $u_*^2/H \sim \nu u_*/\delta_u^2 \Rightarrow \delta_u \sim \sqrt{H\nu/u_*}$. This means that

$$\delta_u \sim \frac{H}{\sqrt{Re_*}} \gg \delta_b \sim \frac{H}{Nu} \tag{26}$$

for $Ra \gg 1$, assuring the self-consistency of the second assumption leading up to (24) (by a factor of $Ra^{1/14}$, which is a large number only for very large Ra). Note also how important the roles of kinetic energy dissipation and the shear boundary layer with the boundary stress u_* are in this scaling theory.

Another way to distinguish these two regimes is in terms of their single-point PDFs for $b'(z = 0)$ (Fig. 8). Note that soft turbulence has an approximate Gaussian distribution, indicating only slight intermittency. In contrast, hard turbulence has an approximate exponential distribution, indicating significant intermittency, as in the regimes of 2D and 3D homogeneous turbulence and shear turbulence, among others. Away from the center of the domain, the PDFs for b' become skewed due to unequal influences of the unequally distant boundaries; nevertheless, the transition from soft to hard turbulence is still evident in the shape of the asymmetric PDFs.

There is another scaling argument due to Kraichnan (1962) based on the hypothesis that ultimately, at high enough Ra, both the momentum and buoyancy boundary layers in (26) will be
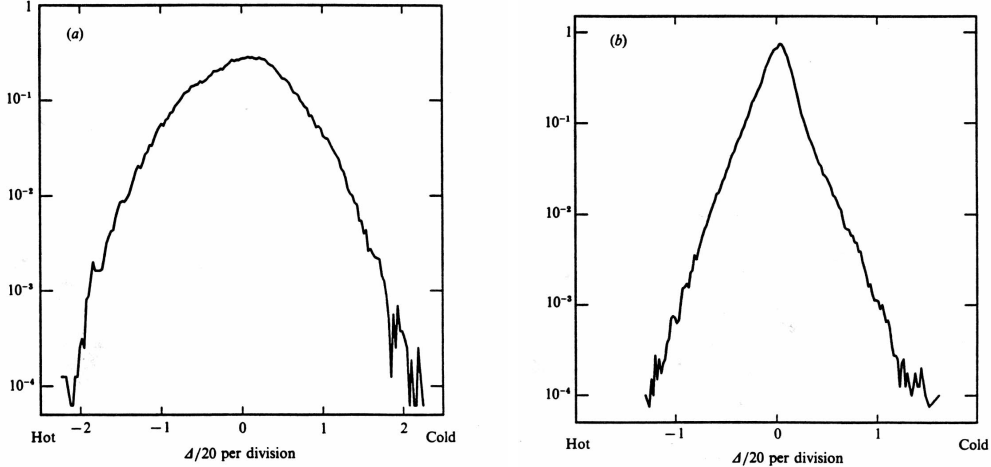
Figure 8: Histograms of the temperature distribution in the center of the domain. (a) Soft turbulence regime, $Ra = 8.4 \times 10^6$. (b) Hard turbulence regime, $Ra = 1.5 \times 10^8$. (Castaing *et al.*, 1989)

fully turbulent with buoyancy advection and conduction of comparable importance; in particular, in the buoyancy boundary layer with an advective length scale of δ_b,

$$u_* \sim \frac{\kappa}{\delta_b} \quad \Rightarrow \quad \frac{\delta_b}{H} \sim Re_*^{-1}Pr^{-1} \tag{27}$$

(thus violating the assumption above of a viscous sub-layer structure for the velocity within the thermal boundary layer that led to (24)). With the Nu relation (16) relating the total buoyancy flux to the buoyancy diffusion across the boundary layer, energy balance (20)-(21) relating the velocity scale and Reynolds number to Nu, and (27) relating δ_b to the velocity scale, we obtain the following scaling relations for the Nusselt and Reynolds numbers as functions of Ra:

$$Nu \sim Pr^{1/2}Ra^{1/2}, \qquad Re_* \sim Pr^{-1/2}Ra^{1/2}. \tag{28}$$

A very simple, alternative derivation of the first relation is to ask which exponents, γ and χ, render the power-law relation, $Nu \sim Pr^{\gamma}Ra^{\chi}$ a statement that $\mathcal{B}$ is indedendent of ν and κ; this yields a unique answer, $\gamma = \chi = \frac{1}{2}$.

This is conceived of as the "ultimate" turbulent regime because purely diffusive and viscous controls of the boundary layers have been exceeded. Howard (1963) showed that Nu has an upper bound $\sim Ra^{1/2}$ as $Ra \to \infty$, consistent with (28). As yet no unambiguous experimental or computational evidence has been found for this relation even though experiments have now reached very large Ra values (but see the final paragraphs of this section). But, *e.g.,* given the self-consistency of the regime (17) demonstrated by (26), this is not necessarily distressing, since it does not require that the ultimate transition occur at any particular value of Ra.

Following the experimental demonstration of hard turbulence with the $Nu[Ra]$ relation in (17), several computational studies showed similar behavior (*e.g.,* Figs. 16-17 below), although they could not achieve such large Ra values as the experiments in liquid helium (Figs. 7-8). The matter appeared settled, at least pending further experiments or computations at higher Ra values
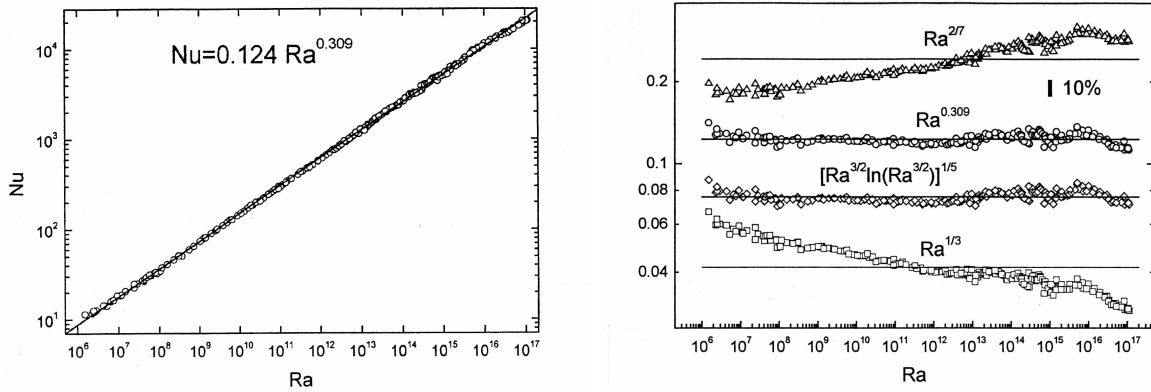
Figure 9: The $Nu - Ra$ correlation at large Ra values. (Left) Log- log plot. (Right) Compensated plots with alternative scaling exponents. (Niemela *et al.*, 2000)
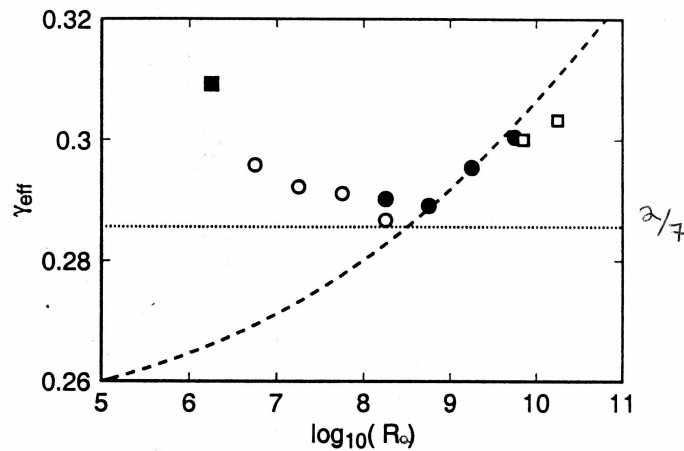

Figure 10: The $Nu - Ra$ correlation at large Ra values, here plotted as a best-fit scaling exponent over local Ra ranges, $\gamma_{eff} = d\log[Nu - 1]/d\log[Ra]$. (Xu *et al.*, 2000)
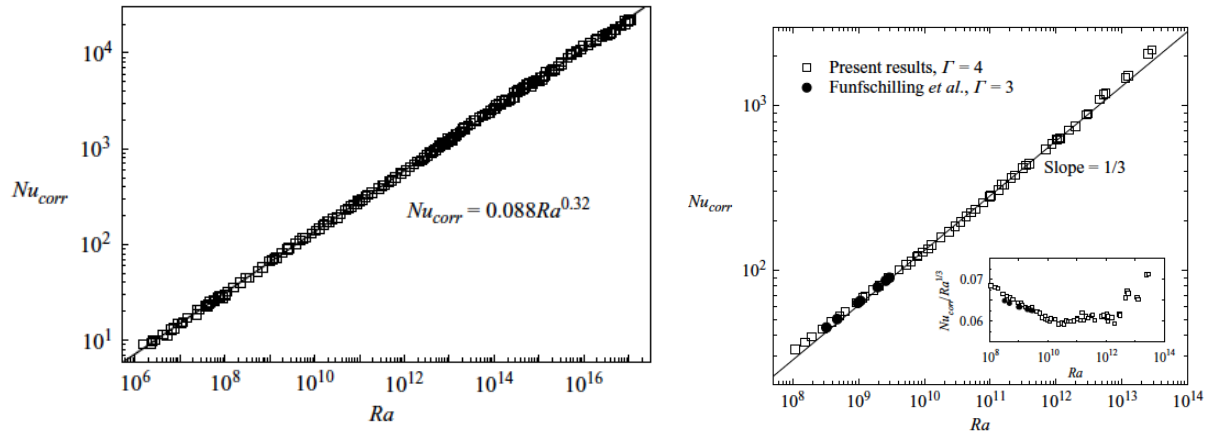
12

Figure 11: The $Nu - Ra$ correlation at large Ra values. The plot on the left is for a domain with horizontal/vertical domain aspect ratio 1/2, and the one on the right is for aspect ratios 3 and 4. (Niemela and Sreenivasan, 2006)
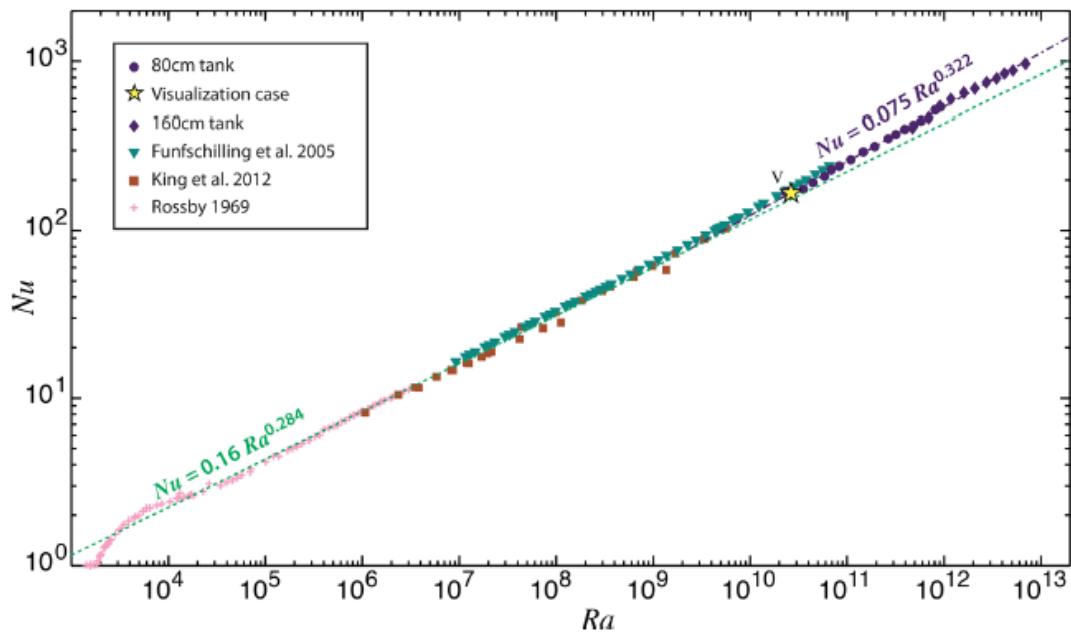

Figure 12: The $Nu - Ra$ correlation at large Ra values. (Cheng *et al.*, 2015)

(*i.e.,* higher than $Ra \approx 10^{13}$). However, quite recently this complacency has been upset by new experimental results. One comes from further experiments in gaseous and liquid helium (Niemela *et al.*, 2000) that span an even larger range of Ra than before (Fig. 9): it shows a good $Nu[Ra]$ power-law relation for Ra values up to $\approx 10^{17}$, but the best-fit power-law exponent is 0.309, which is smaller than $1/3 = 0.333$ yet larger than $2/7 = 0.286$. A principal reason for the disagreement with Fig. 8 is attributed to corrections to the constitutive properties of helium, and these authors even re-process the earlier experiments to show their approximate consistency with the new estimate for the exponent. This is rather unsettling since it is uncertain whether even now the constitutive properties of cryogenic fluids are well enough known to allow reliable interpretation of the results. As yet no theoretical argument has been adduced for the new exponent. The second upsetting new results come from experiments in acetone (Xu *et al.*, 2000), which do not have the constitutive uncertainties of liquid helium. Here the attempt to fit a power-law exponent (Fig. 10) fails to show consistent scaling behavior; instead, there is a range of Ra where the exponent is decreasing — from the value 0.333 in (14) towards a value very close to 0.286 in (17) — but at larger Ra the exponent begins to increase again — approaching a value close to the 0.309 fit in Niemela *et al.* (2000), or possibly even increasing toward Kraichnan's (1962) value of 0.5 at large enough Ra.

At the risk of belaboring this topic, two "final" (or at least more recent) entries into this quest for a "universal" scaling behavior show consider $Nu[Ra]$ relation for laboratory data and power-law fits in Figs. 11-12. They generally support the evidence that there is a soft-turbulence regime at medium-high Ra with $Nu \sim Ra^{1/3}$, a hard-turbulence regime at higher Ra with $Nu \sim Ra^{2/7}$, and a reversion back toward the 1/3 power-law exponent at even higher Ra. Because the $2/7$ regime is rationalized by the importance of a "large-scale" circulation with horizontal flow near the boundary to obtain (25), it is possible that the reversion to a 1/3 regime is associated with the experimental practice of using tall, skinny devices that might suppress the large-scale flow. Finally, efforts to further increase Ra in laboratory devices risk contamination by introducing non-Boussinesq effects into the fluid dynamics.

For now we must consider the matter unresolved, both with respect to the interpretation of the various experiments and the validity of the conception that $Nu[Ra]$ should exhibit a universal scaling behavior in the regime of hard turbulence, never mind whether its exponent, if it exists, might be predicted by a simple phenomenological theory like those presented above. What is not disputed, though, is that there is a regime transition between soft and hard turbulence in buoyant convection that occurs well past the disappearance of any apparent periodicities in the flow structure, *i.e.,* a "bifurcation" within the putative fully developed regime. A recent review of the evidence about the large-Ra regime is Ahlers *et al.* (2009).

Rayleigh-Benard (RB) convection is a rare type of flow that can, in principle, be done under highly controlled laboratory conditions in fully developed turbulence at large Re. Another is Taylor-Couette (TC) shear flow between two concentric, rotating cylinders. Both flows have clearly distinguished interior and boundary layer regions. Eckhardt *et al.* (2007) argues that these two flows should have a very close correspondence in their turbulent behaviors, where Ra has its counterpart in the Taylor number, $Ta \sim L^4(\Delta\Omega)^2/\nu^2$, where L is related to radial distance and $\Delta\Omega$ is the differential angular velocity between the cylinders (*i.e.,* similar to Ek^{-2} with the Ekman number, ν/fL^2, seen previously in the rotating shear boundary layer). The κ and $\Pr$ thermal parameters in RB have corresponding TC parameters related to ν and the cylinder gap size. Chavanne *et al.* (1997) reports a further high-Ra transition in the $Nu[Ra]$ relation in RB that is interpreted as an indication of the ultimate regime predicted by Kraichnan (1962); however, the interpretation

is subtle and others have not yet been able to reproduce it. Quite recently, van Gils *et al.* (2011) reports a similar high-Ta scaling dependence in TC for the torque due to the stress on the surfaces of the cylinders.

In my judgment the ultimate behavior of turbulence as $Re \to \infty$ is still undetermined, although obviously it is an extremely important question in basic physics. The usual Ra and/or Re values of geophysical planetary boundary layers are higher than in these laboratory experiments, so the presumption should be that they are in the ultimate regime, whatever it is in its asymptotic scaling dependencies. The more usual geophysical view is that the surface buoyancy flux $\mathcal{B}$ and/or stress τ are strongly constrained by the larger-scale environment, hence the values of Nu and/or its stress counterpart can be calculated from the known values of ν and κ and the mean vertical profiles, *i.e.,* the scaling behaviors with Ra and/or Ta (or Ek) are not the primary issue, and the turbulent transport will be what it has to be to accommodate the environmental flux and associated Ra and/or Ta values. A deeper view, however, is that the environment and turbulence co-determine each other.
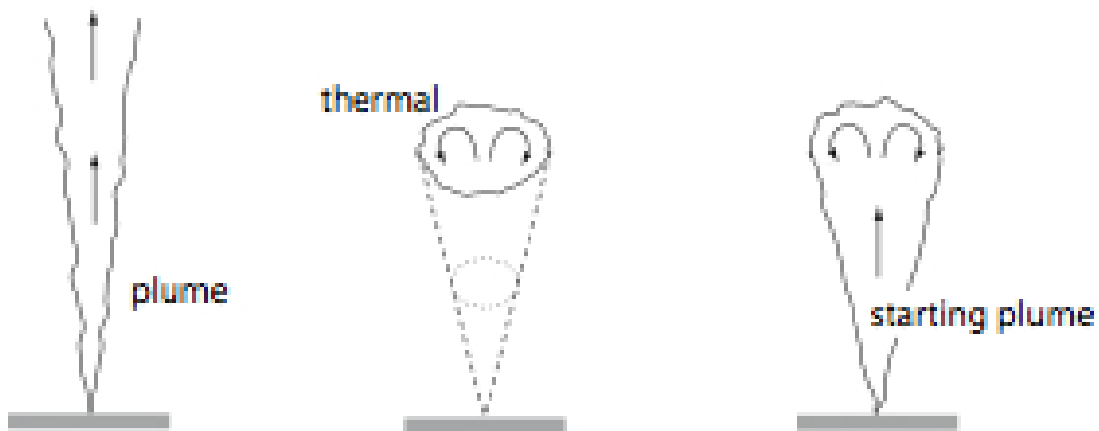
3   Plumes and Thermals

Figure 13: Sketches of a plume, a thermal, and a starting plume following Turner (1973).

An important convective paradigm in the atmosphere is the plumes or the thermals; they are the conceptual building blocks for many models of clouds. Turner (1973) distinguishes between plumes, thermals, and starting thermals as illustrated in Fig. 13. Plumes, or buoyant jets, have a continual — or at least long-lasting — supply of buoyancy at their source (or base), while thermals represent an impulse or bubble of buoyancy which travels through and mixes with the ambient fluid[3]. Because the head, or leading interface, of any plume has the characteristics of a thermal, it proves convenient to introduce the idea of a starting plume when the region of interest is not

---

[3]Popular usage is not always consistent with Turner's definitions. For example, dust devils over hot surfaces in deserts are commonly called thermals.

Figure 14: Shadowgraphs of plumes rising from a heated surface. The upper panel has smaller Ra than the lower one. (Source unknown.)

well separated from the head of the plume. Plumes, thermals, and starting plumes are all driven by density contrasts with the ambient flow, as measured by their density deficit or buoyancy. Plumes driven by a source of momentum and buoyancy are sometimes called forced plumes. In some sense a gravity current can be thought of as a wall-bounded plume. Our focus here is on plumes.

We can visualize the plumes of convection from experiments. The buoyancy patterns in non-rotating plumes, above a heated plate in a laboratory experiment (Fig. 14), resemble mushrooms in cross-sections. Fluid in the upper part of the core of a rising, positive buoyancy anomaly curls over to the sides. This indicates a *vortex ring* structure in the horizontal (*i.e.,* azimuthal) vorticity and the engulfment of ambient fluid as the entrainment mechanism. Neighboring plumes seem to be at most weakly interacting (*i.e.,* in the absence of rotation; Sec. 4). A photograph of a single starting plume is in Fig. 15, where the capping vortex ring is clearly visible.

Plumes are sometimes called buoyant jets, because like jets, which are driven by a constant momentum flux at a point, plumes are driven by a constant buoyancy flux at their source. In the Boussinesq limit this driving flux of buoyancy b can be measured by

$$\mathcal{B}_0 = 2\pi \int_0^\infty wbr\,dr \quad \text{where} \quad b = \left(-g\,\frac{\rho'}{\rho_0} \right), \tag{29}$$

where r measures the distance from the axis of the plume or thermal. Note that in some time interval δt,

$$\frac{\mathcal{B}_0\rho_0\delta t}{g} = -2\pi \int_0^\infty \delta z \rho' r\,dr \tag{30}$$

measures the mass deficit associated with a rising plume. Sinking plumes would correspond to a mass surplus. By definition this deficit (or surplus) is maintained constant in time at the source of a plume, and by mass conservation must be constant with height for plumes rising through an unstratified environment. Because g is fixed, this identifies $\mathcal{B}_0$, z (the distance from the source), and r (the distance from the plume axis) as fundamental parameters of the system. In the limit when other parameters, such as the plume Reynolds number

$$Re = \frac{z^{2/3}\mathcal{B}_0^{1/3}}{\nu}, \tag{31}$$

and the ratio of the distance from the plume to any dimension characterizing its source, are very large, then similarity suggests that solutions of the following form may be relevant:

$$w = \mathcal{B}_0^{1/3} z^{-1/3} f_1\left(\frac{r}{z}\right) \tag{32}$$

$$b = \mathcal{B}_0^{2/3} z^{-5/3} f_2\left(\frac{r}{z}\right). \tag{33}$$

Note that these expressions are singular at the source, but near the source they are not expected to be hold because the similarity assumptions are not valid there. To the extent solutions far from the source obey these similarity forms, they, in effect, define a virtual source or origin for the plume. Experiments confirm this general similarity behavior, with shape functions

$$f_1 \approx 4.7 \exp(-96r^2/z^2) \tag{34}$$

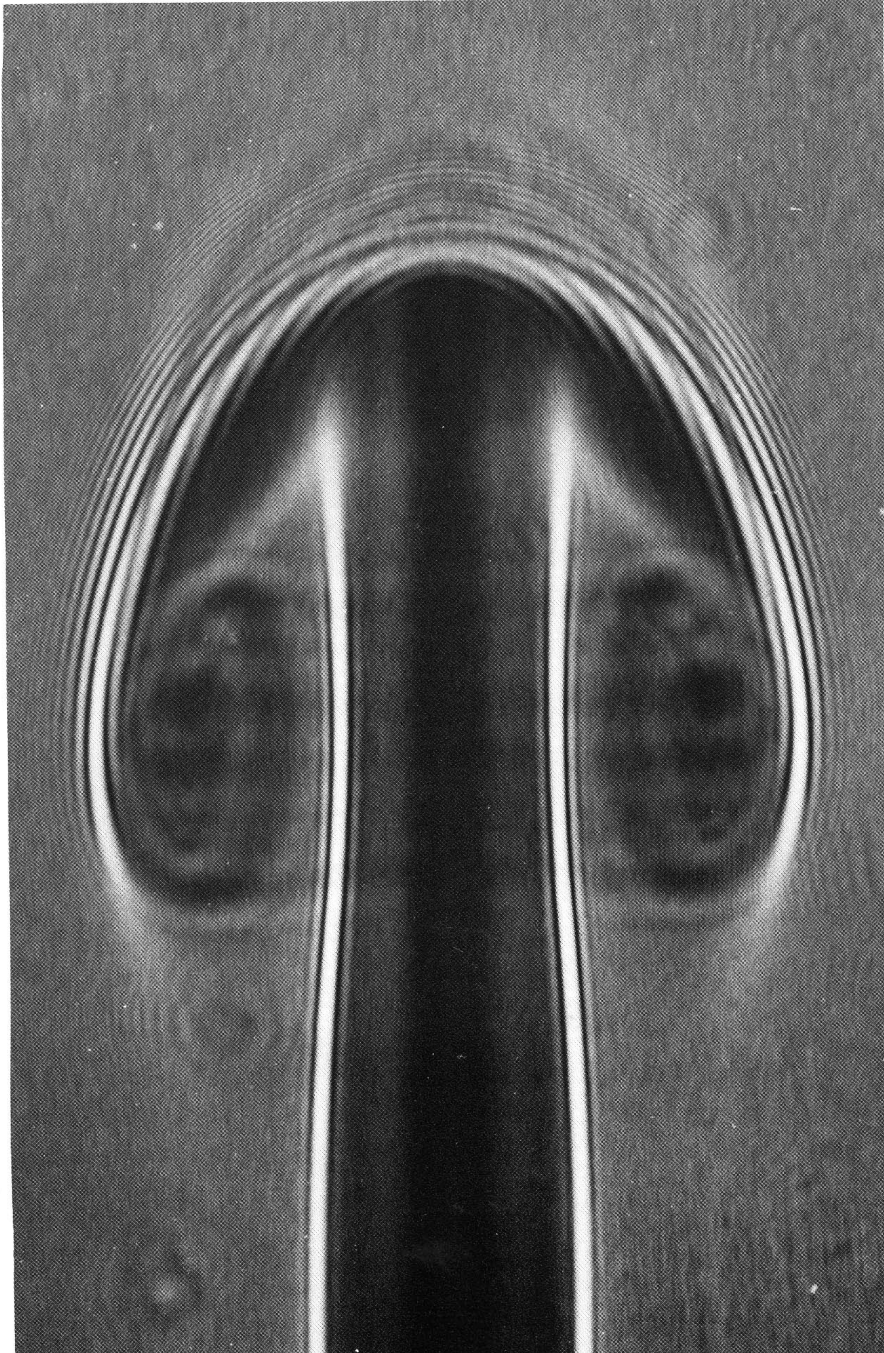$$f_2 \approx 11 \exp(-71r^2/z^2). \tag{35}$$

17

Figure 15: Shadowgraph of an axisymmetric starting plume above a heating source. (From Van Dyke, 1988)

The tendency of the plume to broaden with distance from its source is a statement of its tendency to become turbulent and *entrain* ambient fluid. As a laminar plume accelerates upward, a free shear layer will develop at its boundary with the ambient fluid. This shear layer will be subject to the same types of shear flow instabilities experienced by mixing layers and as a result will "roll up" under the influence of coherent structures or large eddies. As in the free shear layer, these eddies initiate the transition to a fully developed turbulent flow, in this case a turbulent plume. The canonical example of such a process is that of a tendril of smoke emanating from a cigarette. Initially laminar, it develops fluctuations at its boundary some distance above the source. These fluctuations increase in amplitude, and the envelope of smoke becomes turbulent as it spreads into and entrains ambient air. The entrainment process causing the plume to spread is often thought to have two stages: first an engulfment stage, where the large eddies fold in ambient fluid, and then a mixing stage, where the engulfed air is mixed with the turbulent flow through the action of the small eddies. Entrainment is analogous to the process of growth in the thickness of a turbulent shear layer. Entrainment is a common characteristic of turbulence as a particular manifestation of eddy mixing.

For the case of the turbulent plume the entrainment rate is measured by the rate at which the mean plume spreads, which requires some basis for defining the the width of the plume. In much the same way as the velocity deficit can be used to define the depth of a boundary layer, an effective plume width, a, and velocity $\overline{w}$ can be defined on the basis of the mass and momentum fluxes of the actual plume,

$$\overline{w} = \frac{\int_0^\infty w^2(r)r\,dr}{\int_0^\infty w(r)r\,dr} \quad \text{and} \quad a = \left(\frac{2}{\overline{w}} \int_0^\infty w(r)r\,dr \right)^{1/2}. \tag{36}$$

Hence a measures the breadth and velocity a "top-hat" plume with the same mass and momentum fluxes as an actual plume. A top-hat plume refers to the idealization,

$$w(z) = \begin{cases} \overline{w}(z) & 0 \leq r < a \\ 0 & \text{otherwise.} \end{cases} \tag{37}$$

Substituting for $w(r)$ from (32) and (34) yields

$$\overline{w} = 2.35 \left(\frac{\mathcal{B}_0}{z} \right)^{1/3} \quad \text{and} \quad a = \frac{z}{7}. \tag{38}$$

That is, the plume diameter, $2a$, is comparable to the plume height, $H \sim z$, indicating that there is approximate horizontal-vertical isotropy in plumes and, more generally, in convection. We note by these definitions for a Gaussian plume profile that the amplitude prefactor completely determines the plume strength while the prefactor in the exponent determines its width.

The mass flux of a plume $M = \rho_0 \overline{w}(\pi a^2)$ is a fundamental quantity, which is often used to quantify the entrainment. Indeed, for a top-hat plume

$$\frac{z}{M} \frac{dM}{dz} = \frac{5}{3}. \tag{39}$$

This can be integrated to give a solution for all $z > z_0$,

$$M = M_0 \left(\frac{z}{z_0} \right)^{5/3}. \tag{40}$$

Thus, lateral mixing and entrainment cause an increasing upward mass transport with height, which in turn has to be mass-balanced by descending return flows around the plume periphery.

The fractional entrainment rates, and expressions of the form (39) are often used as a foundation for the study of clouds, as well as for their parameterization in atmospheric models.

4   Rotating Convection

Convection can also be influenced by Earth's rotation. A measure[4] of when this occurs is a convective Rossby number, defined by

$$ Ro = \frac{B^{1/2}}{H^{1/2}f} \quad \text{or} \quad \frac{|\mathcal{B}|^{1/3}}{H^{2/3}f} \, . \tag{41} $$

We can make an estimate of Ro for oceanic sub-polar deep convection using the following values: $f = 10^{-4}$ s^{-1}, $B = \alpha g \Delta T$, $\alpha = 0.5 \times 10^{-4}$ K^{-1}, $g = 10$ m s^{-2}, $\Delta T = 0.05$ K, and $H = 2500$ m. The result is $Ro = 1$. A larger buoyancy difference or flux, or a shallower convective depth, will have a larger Ro, hence a weaker rotational influence. For the atmosphere, the typical values of $\alpha = 1/T \approx 3 \times 10^{-3}$ K^{-1} and $\Delta T \approx 5$ K are large enough so that even with $H = 10^4$ m (*i.e.,* the full tropospheric depth), $Ro \gg 1$ and the rotational influence is small (*i.e.,* with respect to Earth's rotation rate f, whereas a rotating storm, like a thunderhead or hurricane may provide a local rotation rate that does influence its internal convection). Another way to express the influence of rotation is through a horizontal length scale, L_{rot} — somewhat analogous to the baroclinic deformation radius for a stably stratified fluid, $R_d = NH/f$ — defined by the relations $Ro = 1$ and $L_{rot} = H$; *viz.,*

$$ L_{rot} = \frac{B}{f^2} \quad \text{or} \quad \frac{|\mathcal{B}|^{1/2}}{f^{3/2}} \quad \Rightarrow \quad Ro = \left(\frac{L_{rot}}{H} \right)^{1/2} \text{or} \left(\frac{L_{rot}}{H} \right)^{2/3} . \tag{42} $$

If a convective plume is emitted from a buoyantly forced boundary with $L < L_{rot}$, it will tend to grow in size through *entrainment* of the ambient fluid it passes through, unless it grows as large as L_{rot}, after which it will cease to entrain nor will it grow any further laterally.

Numerical solutions for the rotating Rayleigh-Benard problem are shown in Figs. 15-18. The mean buoyancy profile (Fig. 5, right panel) remains gravitationally unstable in the interior even as $Ra \to \infty$, and the buoyancy boundary layer becomes increasingly thin. This behavior is unlike that in non-rotating convection where the mean buoyancy gradient becomes very small or even

---

[4]A different but equivalent measure is based on the Taylor number,

$$ Ta = \left(\frac{fH^2}{\nu} \right)^2 , $$

which is approximately the same as the inverse of the Ekman number, often used for the Ekman boundary layer. In combination with Ra, Ta is related to the Rossby number (41) by

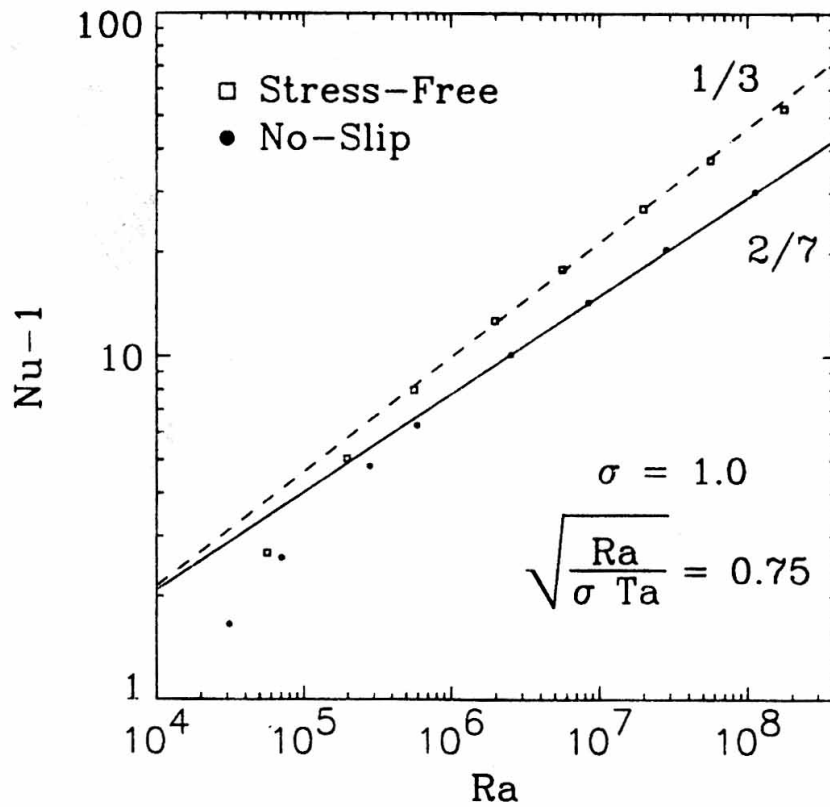$$ Ro = \left(\frac{Ra}{Pr\,Ta} \right)^{1/2} . $$

20

Figure 16: The $Nu - Ra$ correlation at large Ra values for moderately-rotating convection with $Ro = 0.75$. The different symbols are for different boundary stress conditions. The solid and dashed lines correspond to scaling exponents of 2/7 and 1/3, respectively. (Julien *et al.*, 1996)
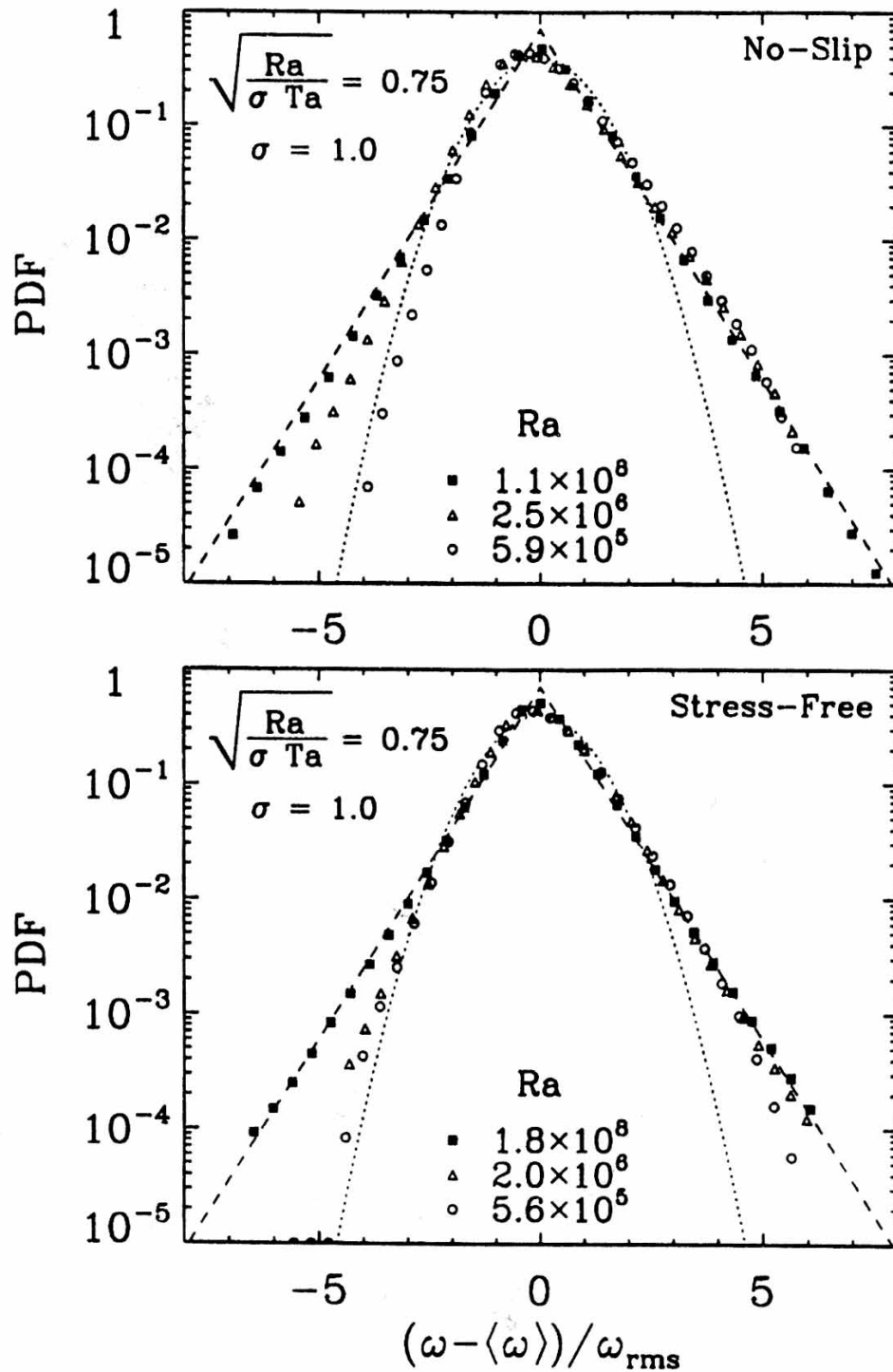
Figure 17: PDFs for vertical vorticity ζ_z in rotating convection for different boundary stress conditions. Dashed and dotted lines correspond to exponential and Gaussian distributions, respectively. (Julien *et al.*, 1996)

slightly positive in the interior (*cf.,* Fig. 5, left panel). It is an indication that rotating plumes do not retain their core fluid as well during the transit from one boundary layer region to the other: they are leakier, which is also consistent with their having less efficient entrainment. Nevertheless, the transitions to hard turbulence at large Ra also occur in rotating convection, as indicated by both the $Nu(Ra)$ law in (17) (Fig. 16) and the exponential form of the b' PDF (Fig. 17). It is of particular interest that alternative solutions with a free-slip (*i.e.,* no stress) velocity boundary condition do not exhibit the hard-turbulence $Nu(Ra)$ dependence, but rather have the soft-turbulence form (14); this gives support to the scaling theory in Sec. 2 based on the important roles played by $u_* \neq 0$. Notice, however, that the range of Ra in Fig. 16 is very small compared to those in the experiments (Figs. 8 and 9-10), so we cannot use the apparent computational confirmation of the scaling relation as sufficient evidence to resolve the experimental controversies.

We can visualize the plumes of rotating convection from numerical simulations. In contrast to non-rotating plumes (Sec. 3), rotating plumes show vortex columns of cyclonic vertical vorticity; this vorticity arises from the environmental rotation being concentrated and intensified by the vortex stretching during the boundary-layer convergence and plume emission process (Figs. 18-19). Thus, we can expect there to be important line vortex interactions, as in 2D homogeneous turbulence, among the plumes of rotating convection. This is consistent with the occasional loss of core material from the plumes, hence the incomplete buoyancy transport across the domain, hence a statically unstable $\bar{b}(z)$ profile as in Fig. 5, right panel. Note that the degree to which the flow pattern is dominated by plumes, as opposed to domain-filling convection cells, increases with increasing Ra values. A detailed analysis of the structure and statistical properties of plumes in rotating convection is in Julien *et al.* (1999).

A different regime occurs in the limit of very strong rotation, $Ro \rightarrow 0$. The results of an early laboratory study by Rossby (1969) stood apart from the lines of research described above, and recently King *et al.*, (2009) reconciled these two regimes. When the Ekman-layer momentum boundary layer thickness, $\delta_{Ek} \sim (\nu/f)^{1/2} = H Ek^{-1/2}$ (*Shear Turbulence*), becomes thinner than the buoyancy boundary layer thickness in the hard-turbulence regime, $\delta_b \sim H Ra^{-2/7}$, then the scaling behavior changes to a much steeper law, empirically fit as

$$Nu \sim Ra^{6/5} \tag{43}$$

(Fig. 20), which as yet does not have a theoretical rationalization. The evidence for this is shown in the $Nu - Ra$ diagram in Fig. 20. Decreasing Rossby number generally stabilizes the convection, in particular by increasing the critical $Ra_{cr}(Ro)$ value for convection onset. Furthermore, an increase in $Ra \sim B$ by increasing B also causes an increase in $Ro \sim B^{1/2}$. Therefore, for strongly rotating flows with $Ro \ll 1$ and increacsing B, there only a narrow experimental window for increasing Ra above Ra_{cr} before reaching the limit of the rotating regime where $Ro \geq 1$.

Rewriting the strongly-rotating regime condition in terms of Ro using (41), we obtain

$$
\begin{aligned}
\delta_{Ek} &\lesssim \delta_b \\
\Rightarrow \quad Ro &\lesssim Pr^{-1/2} Ra^{-1/14} .
\end{aligned}
\tag{44}
$$

The small exponent for Ra implies that the requisite Ro values do not need to be too small even when Ra is quite large. Evidently, the moderately-rotating results in Fig. 16 have not yet crossed into the strongly-rotating regime in Fig. 20, even though they do have a small-enough Ro value to show significant departures from non-rotating convection in other attributes. (In retrospect we, the
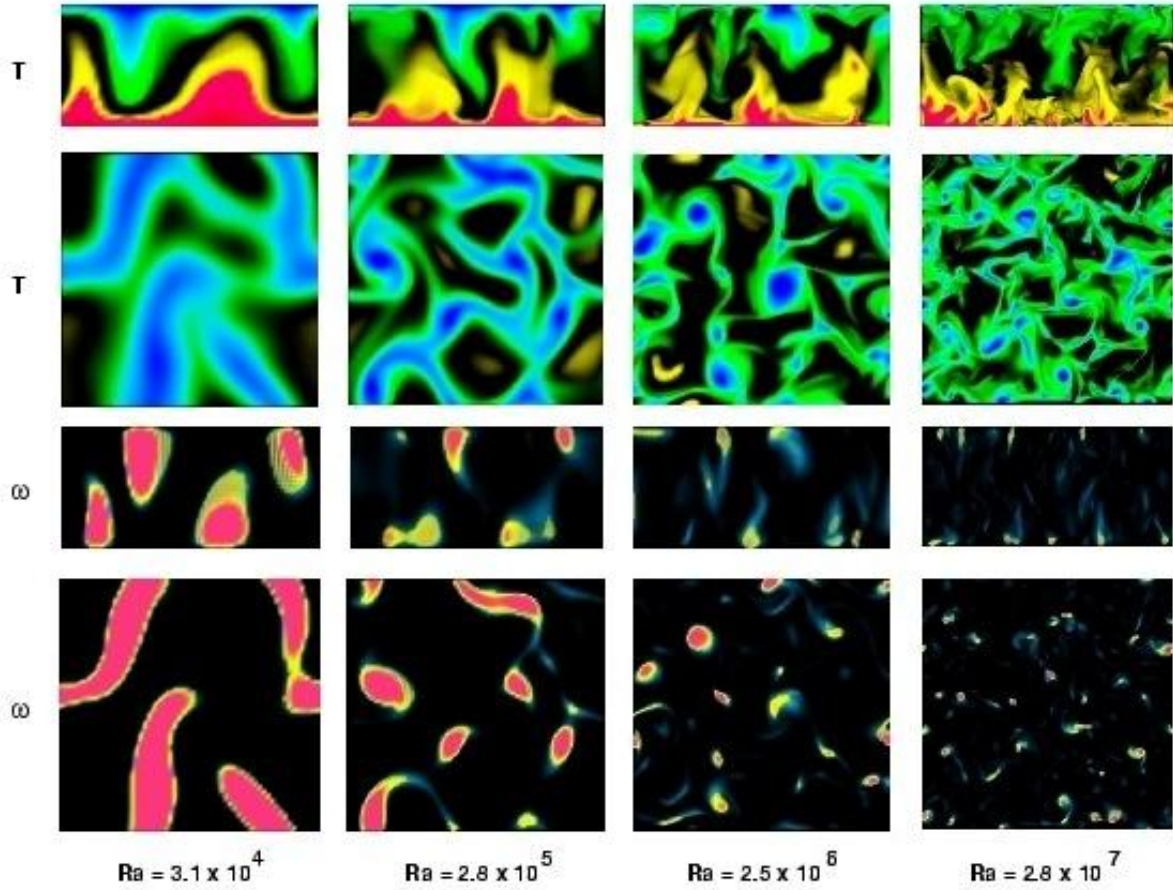
Figure 18: Side- and top-view snapshots of T and ζ_z in a computational simulation of rotating Rayleigh-Benard convection with $Ro = 0.75$ at several different Ra values. Note the transition from convection cells to plumes as Ra increases, and note the cyclonic swirl (*i.e.*, $\zeta_z/f > 0$) in the plumes. (Julien *et al.*, 1996)
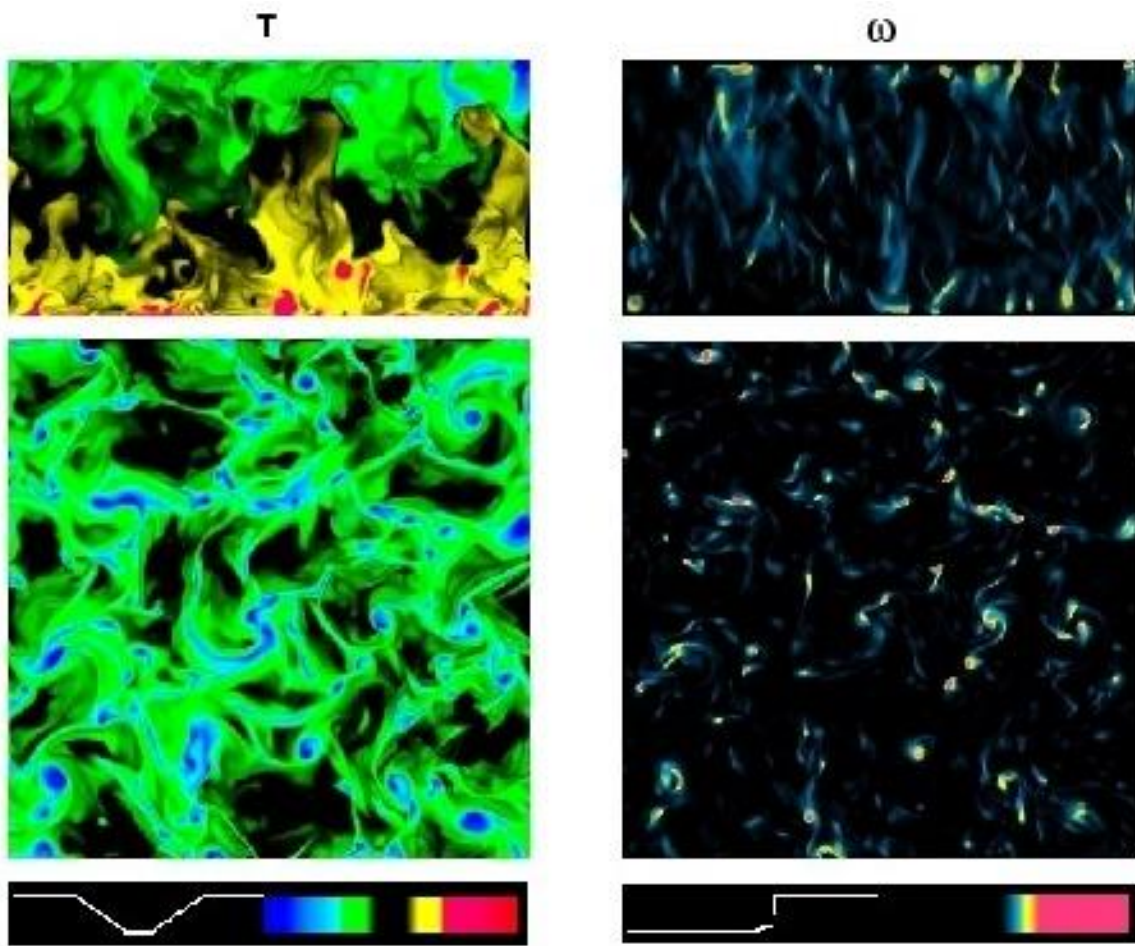
Figure 19: Side- and top-view snapshots of T and ζ_z in a computational simulation of rotating Rayleigh-Benard convection with $Ro = 0.75$ at a rather large value of $Ra = 1.1 \times 10^8$. (Julien *et al.*, 1996)
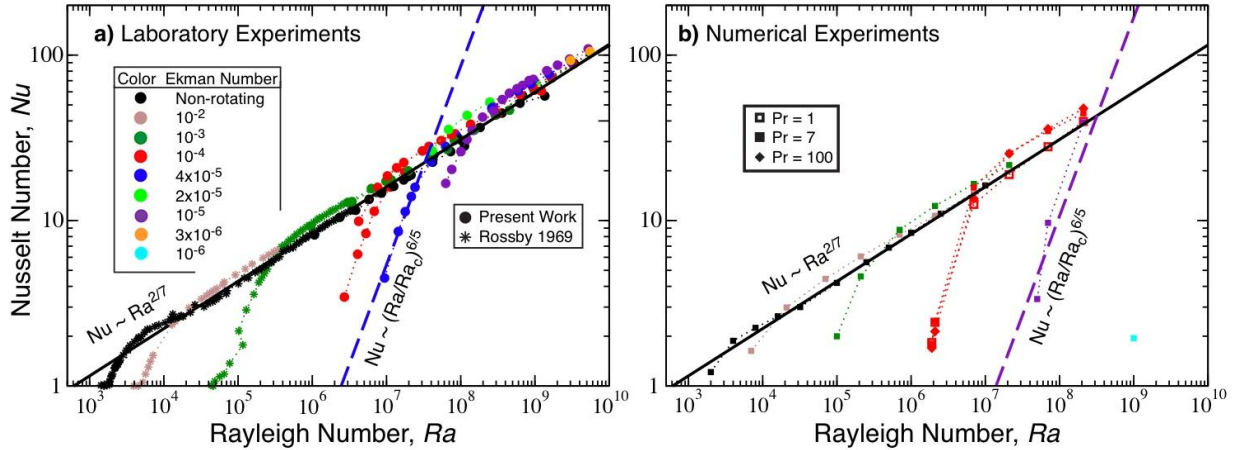
25

Figure 20: Nusselt number, Nu, versus Rayleigh number, Ra, for (a) laboratory experiments and (b) numerical simulations. Non-rotating convection in laboratory experiments yields $Nu \propto Ra^{2/7}$ (solid black lines). Dashed lines represent the rotationally-controlled scaling law $Nu \propto Ra^{6/5}$. (King *et al.*, 2009)

authors of the former study, can feel some chagrin that we did not pursue cases with even smaller Ro values.)

Recently, Julien *et al.* (2015) produced an asymptotic theory as $Ro \rightarrow 0$ that yields, as the leading-order "reduced" dynamics in the interior, a rather exotic vertically non-hydrostatic and horizontally geostrophic momentum balance. As a function of Ra it exhibits the regime transitions illustrated in Fig. 21. It is a singular perturbation theory, with the boundary layer structure as indicated in Fig. 22. The theory seems well confirmed by computational solutions and computational experiments (Plumley *et al.*, 2016). For stress-free top and bottom boundaries, its heat flux scaling is

$$Nu \sim Ra\, Ro\, Pr^{-1/2}\,; \tag{45}$$

i.e., it is much steeply increasing in Ra than non-rotating convection, but it is also steeply decreasing as Ro decreases. Its Ra dependence is less steep than in (43) obtained in experiments for no-slip boundary conditions.

Finally, a very interesting phenomenon has recently been discovered for rapidly rotating convection at high Ra and small Ro, *viz.,* the emergence of large scale, barotropic vortices aligned with gravity (Figs. 23-24). Thus far, the evidence for them comes from numerical simulations, with laboratory experiments now being planned. From initial convective onset of small-scale, 3D motions at early time, the flow exhibits a progressive inverse energy cascade until, at late time, the spectrum peak is near the domain scale and develops into large-scale vortices. There is an approximate equipartition between barotropic and baroclinic kinetic energies, with more barotropic energy at the larger scales and primarily in the coherent vortical flows. Interestingly, the horizontal kinetic energy spectrum has a $\sim k^{-3}$ shape at large scales and a $\sim k^{-5/3}$ at the more obviously convective smaller scales, thereby qualitatively matching the atmospheric spectrum at the tropopause but in a very different dynamical regime and thus probably for very different reasons. The large-scale vortices arise in convection with either stress-free or no-slip boundary conditions, but they are more
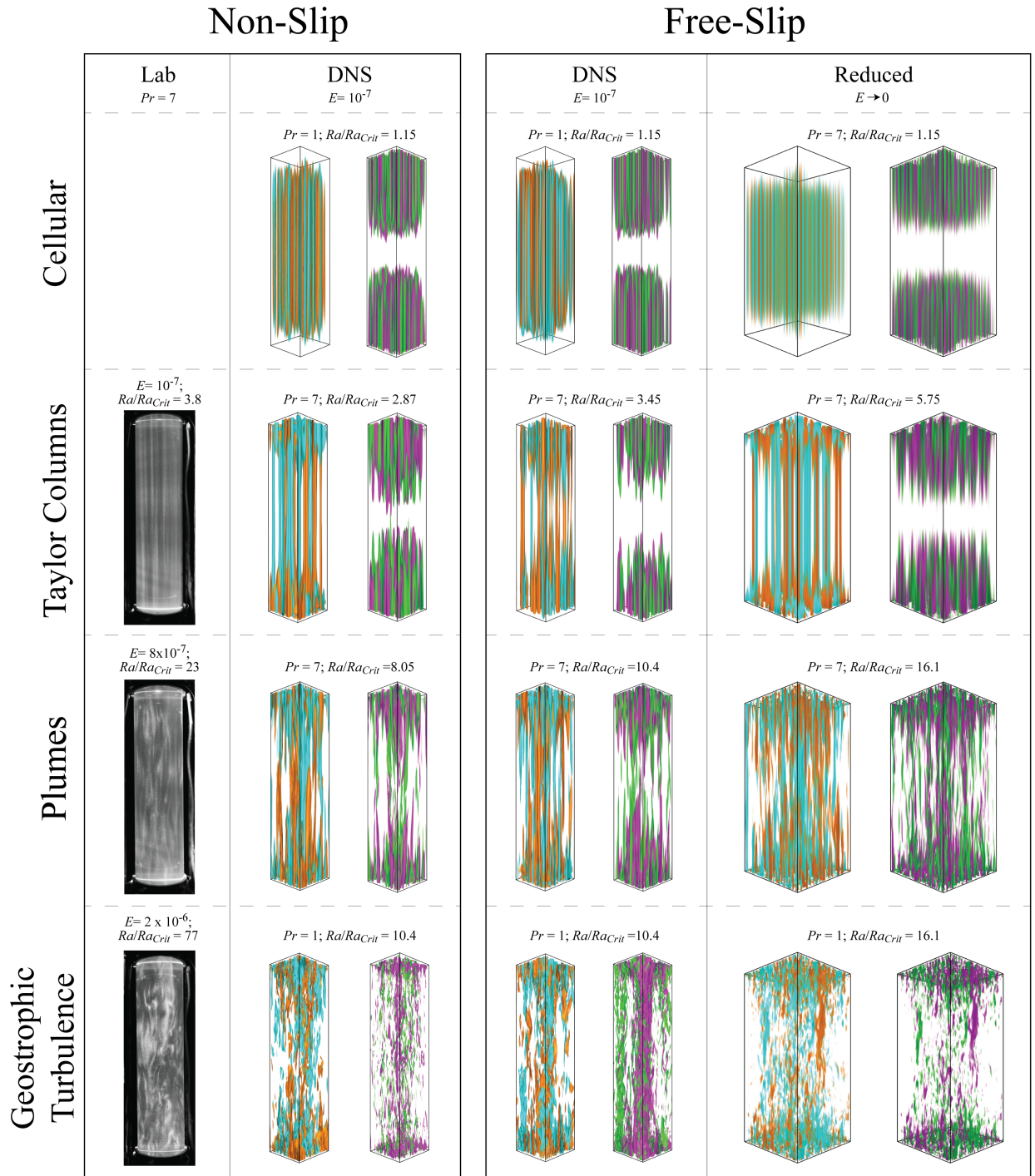
Figure 21: Comparisons between laboratory experiments, DNS, and NH-QGE (the asymptotic non-hydrostatic, "quasigeostrophic" equations) of flow morphologies of rotationally constrained Rayleigh-Benard convection. As Ra (here normalized by its critical value for the first instability of a conducting state) increases, the flow transitions from cellular, convective Taylor columns, plumes, and geostrophic turbulent regimes. (Julien *et al.*, 2015)
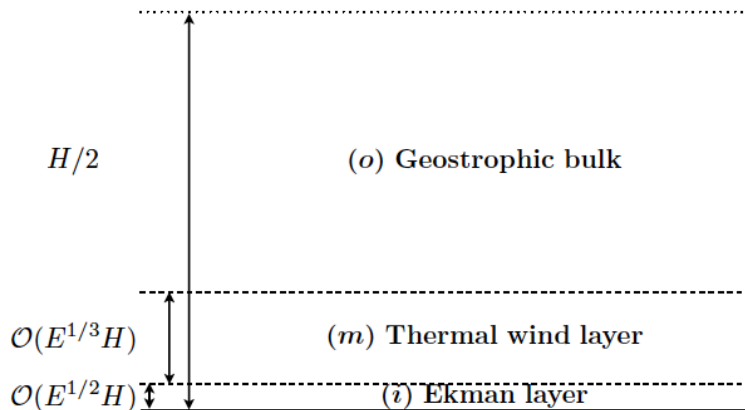
Figure 22: Schematic of the three distinct regions that arise in rapidly rotating Rayleigh-Benard convection with no-slip bounding plates. The half layer [0, H/2] is illustrated with (o) outer region, (m) middle region, and (i) inner region each characterized by distinct balances in the governing equations. The outer region is characterized by geostrophically balanced convection. The inner region consists of a classical, linear Ekman layer. To satisfy the perfectly conducting thermal boundary conditions employed in the present work, a middle diffusive thermal-wind layer is necessary (*i.e.,* with hydrostatic balance, in contrast to the bulk layer that is non-hydrostatic and has strong buoyant accelerations). (Julien *et al.*, 2015)

dominant in the former case. This phenomenon is potentially of great relevance for rapidly rotating planets and stars.

This asymptotic model is referred to by its creators as quasi-geostrophic and the regime illustrated in Figs. 21, bottom row, and 23-24 as geostrophic turbulence. Later in the *Geostrophic Turbulence* notes, we will see that this terminology arose — and are still mostly used — in the context of Earth's stably stratified ocean and atmosphere in reference to large-scale flows with $Ro \ll 1$, $Fr_v \ll 1$, and hydrotstatic vertical momentum balance.

5   Penetrative Convection

In the ocean and atmosphere, almost all convection arises from a destabilizing buoyancy flux on only one side of the fluid layer, usually is at the land surface or the air-sea interface. On the other side of the destabilizing flux, the convective motions are *penetrative*, with their vertical extent limited by an *inversion* layer of stably stratified fluid. In this situation, the convective turbulence is usually temporally developing, and it is quite rare for it to reach an equilibrium state where the buoyancy flux through the inversion layer is equal to the instigating destabilizing flux at the surface. In the atmospheric troposphere the inversion usually lies above the convection, either at the interior edge of the PBL, or at the top of a cumulus cloud field, or at the tropopause that marks the start of the stratosphere. In the ocean, the inversion usually lies below the convection at the interior edge of the PBL, although in shallow water, and even occasionally in deep water, it can reach all the way to the solid bottom. In the atmosphere convection is often influenced by water phase changes (*e.g.,* the latent heat released by condensation, or alternatively the cooling caused by
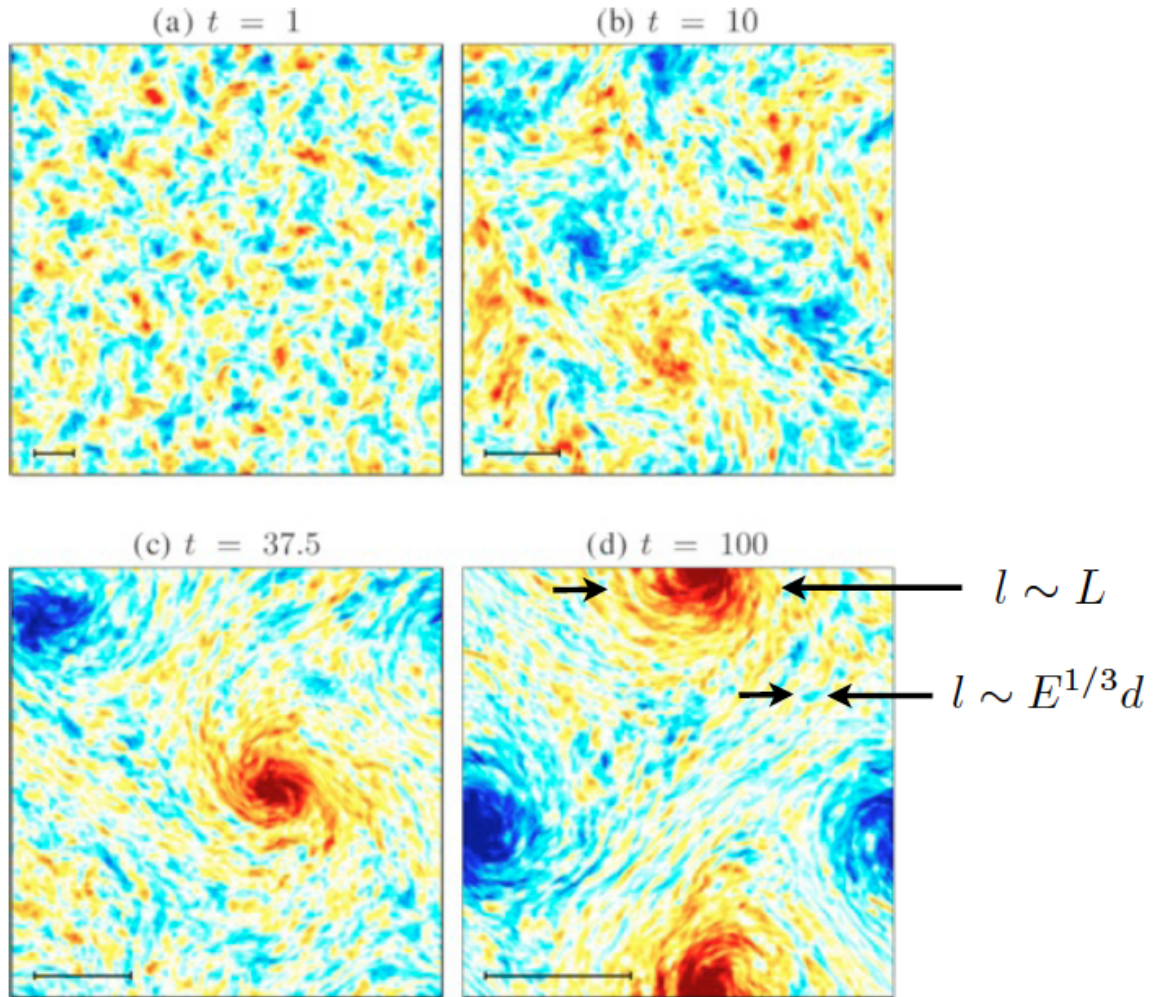
Figure 23: Instantaneous horizontal plots of vertically averaged vertical vorticity at successive times in rapidly rotating Rayleigh-Benard convection. Large-scale vortices develop out of small-scale convective turbulence. Two horizontal scales are evident at late time: a smaller scale $\ell \sim E^{1/3}L$ for the convective plumes, where L is the domain size and $E = \nu/fH^2$ is the Ekman number that is small when f is large, and a larger size for the vortices with $\ell \sim L$. Although not obvious here, the cyclonic vortices are stronger than the anticyclonic ones. (Rubio $et~al.$, 2014)
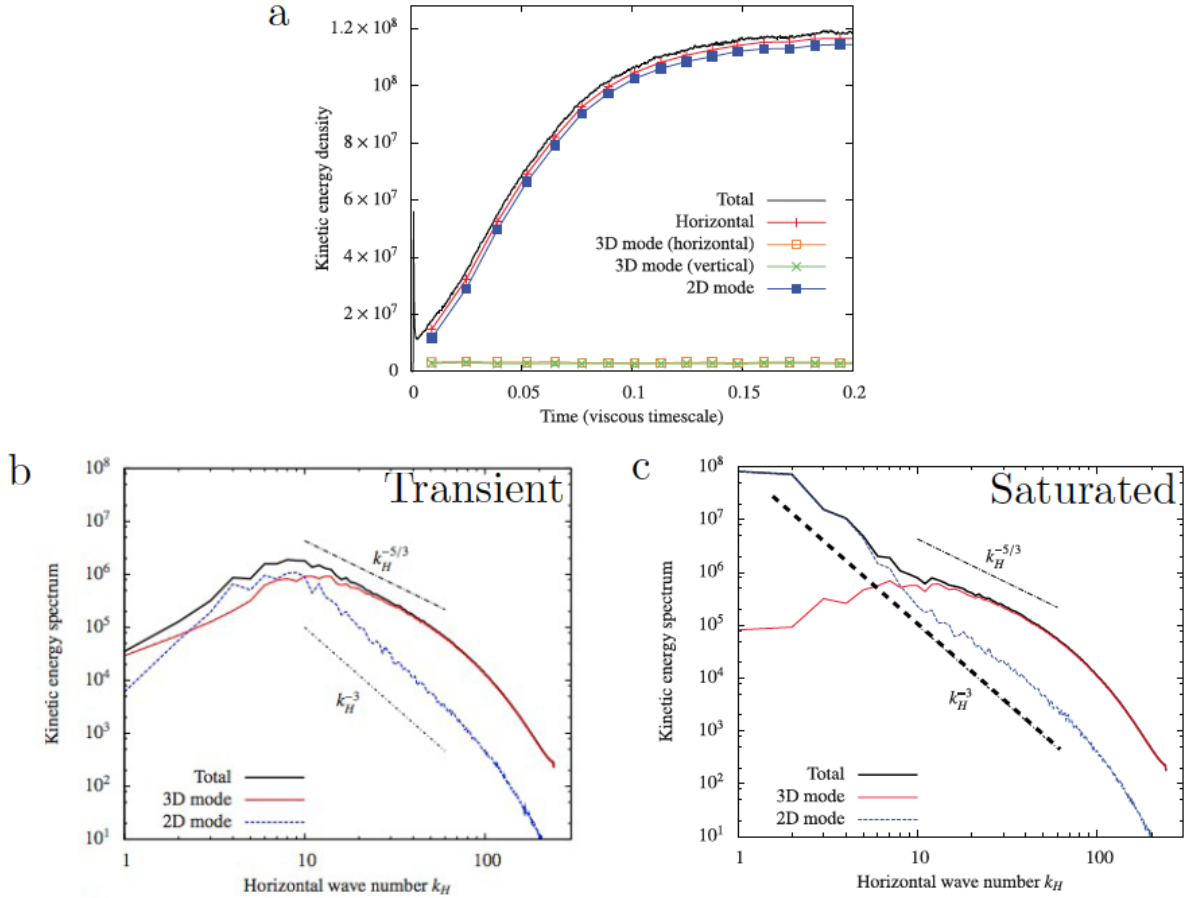
Figure 24: Rapidly rotating convection: (a) Kinetic energy, and (b)-(c) early and late horizontal spectra of kinetic energy, with a decomposition of the velocity into the barotropic (2D) and baroclinic (3D) components, and a further decomposition of the latter into horizontal and vertical flow components. For comparison, power laws of $k_H^{-5/3}$ and k_H^{-3} are drawn, suggestive of a forward energy cascade for the baroclinic modes and a forward enstrophy cascade for the barotropic modes. (Favier *et al.*, 2014)
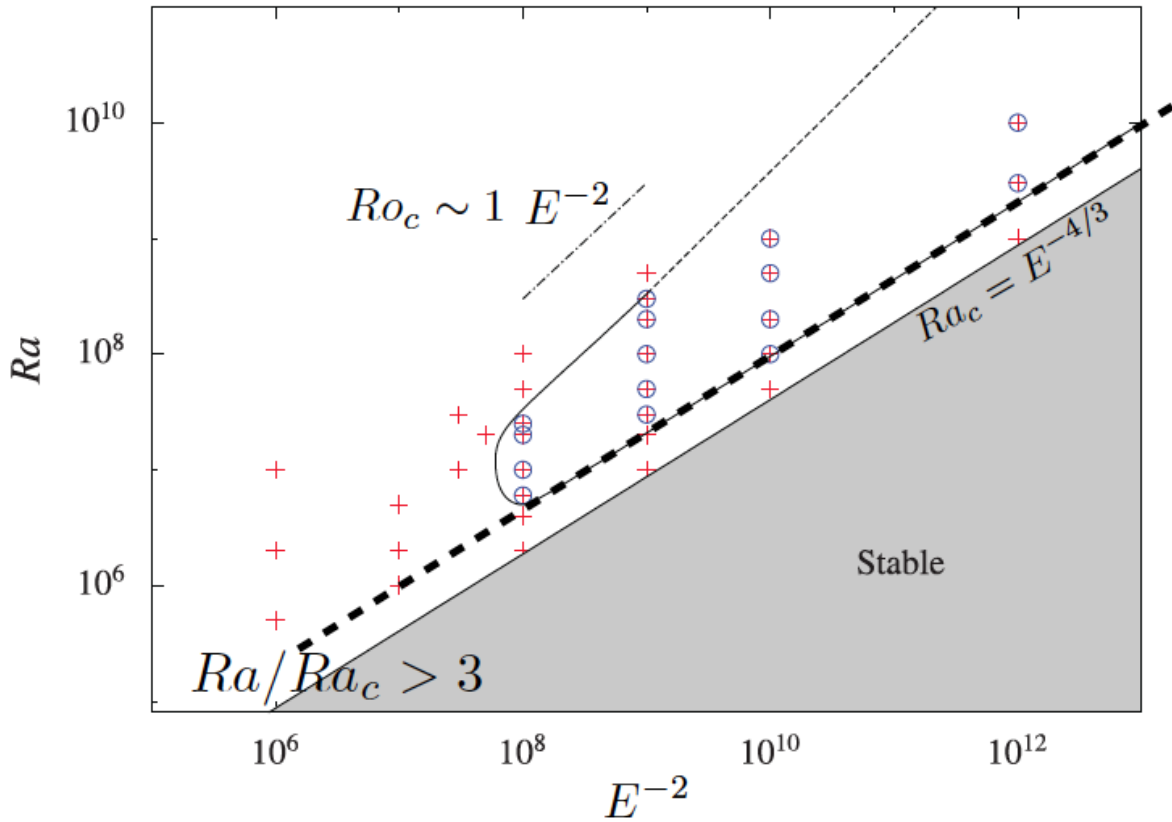
Figure 25: Regime diagram for a set of numerical simulations in rotating turbulent convection. The regime of large-scale vortices occurs for large Ra, Ra much larger than the linear-instability critical value Ra_c, rapid rotation ($E \ll 1$), and Ro less than a critical value of around one, which occurs when $Ra \sim E^{-2}$. The bare plus signs show turbulent cases without large scale vortices, and the circled plus signs show cases with them. (Favier *et al.*, 2014)

evaporation or sublimation of water or ice droplets), but this is not a topic we will address in these lectures. Later we will discuss convective *Planetary Boundary Layers*, a regime of penetrative convection when the surface buoyancy flux is destabilizing.

6   Geophysical Convection

The chapter closes with the brief mention of two other types of convective turbulence found in geophysical flows.

Horizontal Convection: The thermohaline circulation results from surface buoyancy flux differences in heat and freshwater, primarily between tropical and polar regions. This is idealized as horizontal convective turbulence, in contrast to the vertical flux forcing in Rayleigh-Benard convection. It gives rise to a global circulation pattern that contributes importantly to climate heat balance. Paparella and Young (2002) proved an "anti-turbulence theorem" that there is an upper bound on the dissipation rate ε for a flow forced only with a specified surface temperature distribution, and that this bound becomes vanishingly small as $\nu, \kappa \to 0$ (*i.e., $Ra \to \infty$*), *i.e.,* the Kolmogorov regime does not occur. This is interpreted as an indication that the thermohaline circulation, to achieve the strength observed in nature, requires extra sources of turbulent energy from the wind- and tide-driven circulations, hence extra dissipation and mixing, to be as strong and extend as deeply as it is observed to do. However, Scotti and White (2011) argued that the criterion leading to the anti-turbulence theorem is too restrictive and that, based on certain statistical properties of the velocity gradient tensor which are common to all known turbulent flows, horizontal convection is in fact turbulent for all Ra. Barkan *et al.* (2013) demonstrates that, with rotation, the geostrophic circulation that develops in horizontal convection becomes unstable by baroclinic instability and supports fully developed turbulence with finite ε at large Ra. This is not to say that wind and tide influences are unimportant for the real thermohaline circulation, but only that they are not deductively essential.

Convection as $Re \to 0$: In Earth's interior the magma in the mantle is convectively forced by the heat flux from the core to the surface and cooling of the upper mantle from radioactivity and secular cooling. The magma is s highly viscous fluid that extends to about 30 km below the surface, and deeper the motions occur by subsolidus convection. This poses the idealized problem of vertical convection with large Ra and small Re, hence large Pr. Turbulence still occurs in this limit (Breuer and Hansen, 2009).

Readings

Secs. 6.1 and 6.3 in Turner (1973) [plumes and thermals]

References

Ahlers, G., D. Lohse, 2009: Heat transfer and large scale dynamics in turbulent Rayleigh-Benard convection. *Rev. Modern Physics* **81**, 503-537.

Barkan, R., K.B. Winters, and S.G. Llewellyn Smith, 2013: Rotating horizontal convection. *J. Fluid Mech.* **723**, 556-586.

Boffetta, G., A. MAzzino, and S. Musacchio, 2016: Rotating Rayleigh-Taylor turbulence. *Phys. Rev. Fluids* **1**, 054405.

Breuer, M. and U. Hansen, 2009: Turbulent convection in the zero Reynolds number limit. *Europhys. Lett.* **86**, 24004.

Castaing, B., G. Gunaratne, F. Heslot, L., Kadanoff, A. Libchaber, *et al.*, 1989: Scaling of hard thermal turbulence in Rayleigh-Benard convection. *J. Fluid Mech.* **204**, 1-30.

Chandrasekhar, S., 1961: *Hydrodynamic and Hydromagnetic Stability*, Oxford.

Chavanne, X., F. Chilla, B. Castaing, B. Hebral, B. Chabaud, and J. Chaussy, 1997: Observation of the ultimate regime in Rayleigh-Benard convection. *Phys. Rev. Lett.* **79**, 3648-3651.

Cheng, J.S. S. Stellmach, A. Ribeiro, A. Grannan, E.M. King, and J.M. Aurnou, 2015: Laboratory-numerical models of rapidly rotating convection in planetary cores. *Geophys. J. International* **201**, 1-17.

Eckhardt, B. S. Grossman, and D. Lohse, 2007: Torque scaling in turbulent Taylor-Couette flow between independently rotating cylinders. *J. Fluid Mech.* **581**, 221-250.

Emanuel, K., 1994: *Atmospheric Convection*. Oxford Press.

Favier, B., L.J. Silvers, and M.R.E. Proctor, 2014: Inverse cascade and symmetry breaking in rapidly rotating Boussinesq convection. *Phys. Fluids* **26**, 096605.

van Gils, P.M., S.G. Huisman, G.W. Buggert, C. Sun, and D. Lohse, 2011: Torque scaling in turbulent Taylor-Couette flow with co- and counter-rotating cylinders. *Phys. Rev. Lett.* **106**, 025402.

Howard, L.N., 1963: Heat transport by turbulent convection. *J. Fluid. Mech.*, **17**, 405-432.

Julien K., S. Legg, J.C. McWilliams, and J. Werne, 1996: Rapidly rotating turbulent Rayleigh-Benard convection. *J. Fluid Mech.* **322**, 243-273.

Julien, K., S. Legg, J.C. McWilliams, and J. Werne, 1999: Plumes in rotating convection. Part 1. Ensemble statistics and dynamical balances. *J. Fluid Mech.* **391**, 151-187.

Julien, K., J.M. Aurnou, M.A. Calkins, E. Knobloch, P. Marti, S. Stellmach, and G.M. Vasil, 2015: A nonlinear composite reduced model for rotationally constrained convection with Ekman pumping. *J. Fluid Mech.*, submitted.

King, E.M., S. Stellmach, J. Noir, U. Hansen, and J.M. Aurnou, 2009: Boundary layer control of rotating convection systems. *Nature* **457**, 301-304.

Kraichnan, R.H., 1962: Turbulent thermal convection at arbitrary Prandtl number. *Physics of Fluids* **5**, 1374-1389.

Malkus, W.V.R., 1954: Discrete transitions in turbulent convection. *Proc. Roy. Soc. London A* **225**, 185-195.

Niemela, J.J., L. Skrbek, K.R. Sreenivasan, and R.J. Donnelly, 2000: Turbulent convection at very high Rayleigh numbers. *Nature,* **398**, 307-310.

Niemela, J.J. and K.R. Sreenivasan, 2006: Turbulent convection at high Rayleigh numbers and aspect ratio 4. *J. Fluid Mech.* **557**, 411-422.

Paparella, F., and W.R. Young, 2002: Horizontal convection is non-turbulent. *J. Fluid Mech.* **466**, 205-214.

Plumley, M., K. Julien, P. Marti, and S. Stellmach, 2016: The effects of Ekman pumping on quasi-geostrophic Rayleigh-Bnard convection. *J. Fluid Mech.* **803**, 51-71.

Rubio, A.M., K. Julien, E. Knobloch, and J.B. Weiss, 2014: Upscale energy transfer in three-dimensional rapidly rotating convection. *Phys. Rev. Lett.* **112**, 144501.

Rossby, H.T., 1969: A study of Benard convection with and without rotation. *J. Fluid Mech.* **36**, 309-335.

Scotti, A., and B. White, 2011: Is horizontal convection really non-turbulent? *Geophys. Res. Lett.* **38**, L21609.

Shraiman, B., and E. Siggia, 1990: Heat transport in high-Rayleigh-number convection. *Phys. Rev. A* **42**, 3650-3653.

Siggia, E., 1994: High Rayleigh number convection. *Ann. Rev. Fluid Mech.* **26**, 137-168.

Turner, J.S, 1973: *Buoyancy Effects in Fluids*. Cambridge Press.

Van Dyke, M., 1988: *An Album of Fluid Motion*. Parabolic Press, Stanford.

Xu, X., K.M.S. Bajaj, and G. Ahlers, 2000: Heat transport in turbulent Rayleigh-Beńard convection. *Phys. Rev. Lett.* **84**, 4357-4360.

Appendix: Rayleigh-Benard Stability Analysis

The starting point of the analysis is the Boussinesq equations linearized about a resting basic state and a potential temperature $\bar{\theta}$ that varies linearly with height,

$$\bar{\theta}(z) \;=\; \theta_0 + \Gamma_0 z \,, \quad \Gamma_0 \;\equiv\; \frac{\theta_1 - \theta_0}{H} \,.$$

The basic state is denoted by overbars. In this situation the linearized Boussinesq vertical momentum and buoyancy equations become

$$\frac{\partial w'}{\partial t} = \frac{-1}{\rho_0}\frac{\partial p'}{\partial z} + g\frac{\theta'}{\theta_0} + \nu\nabla^2 w' \tag{46}$$

$$\frac{\partial \theta'}{\partial t} = -w'\Gamma_0 + \kappa_h \nabla^2 \theta', \tag{47}$$

where ∇^2 is the three dimensional operator, $\partial^2/\partial x^2 + \partial^2/\partial y^2 + \partial^2/\partial z^2$.

We can eliminate the pressure term in the equation for w' above with the help of the continuity equation. Taking the divergence of the three-dimensional momentum equation leads to the scalar balance:

$$\frac{1}{\rho_0}\nabla^2 p' = \frac{g}{\theta_0}\frac{\partial \theta'}{\partial z}, \tag{48}$$

which allows us to eliminate pressure from our system by substitution into the Laplacian of (46). After these manipulations we find that

$$\left(\frac{\partial}{\partial t} - \nu\nabla^2\right)(\nabla^2 w') = \frac{g}{\theta_0}\nabla_h^2\theta' \tag{49}$$

$$\left(\frac{\partial}{\partial t} - \kappa_h\nabla^2\right)\theta' = -w'\Gamma_0, \tag{50}$$

where $\nabla_h^2 \equiv \partial^2/\partial x^2 + \partial^2/\partial y^2$. Assuming separable solutions of the form

$$w' = \hat{W}(z)\exp\left[i(k_x x + k_y y) + \omega t\right] \tag{51}$$

$$\theta' = \hat{\Theta}(z)\exp\left[i(k_x x + k_y y) + \omega t\right], \tag{52}$$

allows us to recast our system of partial differential equations into a system of ordinary differential equations:

$$\left(\frac{d^2}{dz^2} - k^2\right)\left(\frac{d^2}{dz^2} - k^2 - \frac{\omega}{\nu}\right)\hat{W}(z) = \frac{g}{\nu\theta_0}k^2\hat{\Theta}(z) \tag{53}$$

$$\left(\frac{d^2}{dz^2} - k^2 - \frac{\omega}{\kappa_h}\right)\hat{\Theta}(z) = \frac{\Gamma_0}{\kappa_h}\hat{W}(z) \tag{54}$$

where $k^2 = k_x^2 + k_y^2$. Operating on the first equation with the operator $d^2/dz^2 - k^2 - \omega/\kappa_h$ and substituting from the latter equation yields an ordinary differential equation entirely in terms of $\hat{W}(z)$:

$$\left(\frac{d^2}{dz^2} - k^2\right)\left(\frac{d^2}{dz^2} - k^2 - \frac{\omega}{\nu}\right)\left(\frac{d^2}{dz^2} - k^2 - \frac{\omega}{\kappa_h}\right)\hat{W}(z) = \frac{g\Gamma_0}{\nu\kappa_h\theta_0}k^2\hat{W}(z). \tag{55}$$

Note that this equation has units of inverse time and distance. It can be non-dimensionalized with the aid of a length- and time-scale that we choose to be H and H^2/ν respectively. With these scales the non-dimensionalization yields

$$\left(\frac{d^2}{dz^2} - k^2\right)\left(\frac{d^2}{dz^2} - k^2 - \omega\right)\left(\frac{d^2}{dz^2} - k^2 - \omega\,Pr\right)\hat{W}(z) = -k^2\,Ra\,\hat{W}(z), \tag{56}$$

where all quantities should now be interpreted as being the non- dimensional with

$$Ra = -\frac{g\Gamma_0 H^4}{\nu\kappa_h\theta_0} \quad \text{and} \quad Pr = \frac{\nu}{\kappa_h} \tag{57}$$

being non-dimensional parameters called the Rayleigh and Prandtl numbers, respectively.

Thus the problem of the instability of convective flows reduces to a problem in two parameters, Pr and Ra. The first parameter is a property of a fluid while the second is a measure of how hard the system is forced. Thus given a working fluid, only one parameter is free. Conceptually this is a delightful state of affairs as any two flows of a given fluid should be similar in so far as their Rayleigh numbers are similar. Rather than having to study how convection responds to independent variations in the temperature difference between the plates (as measured by Γ_0 versus

Table 1: Critical Rayleigh number as a function of boundary conditions. Adapted from Table 3.1 of Emanuel (1994).

Boundary Conditions	Ra_c	k_c	π/k_c
Free-Slip	658	2.22	1.42
No-Slip	1100	2.68	1.17
Mixed	1708	3.12	1.01

variations in the depth of the convecting fluid, or the strength of the viscosity) all that is necessary is to study the behavior of the flow as a function of the Rayleigh number.

To select physical solutions to (56) we must first choose the appropriate boundary conditions. Altogether we need six conditions. Four conditions are given by the requirement that

$$\hat{W} = \hat{\Theta} = 0 \quad \text{at} \quad z = 0,\, 1, \tag{58}$$

which is the mathematical expression of the idea that our boundaries are rigid, flat, and perfectly conducting. The remaining two boundary conditions are on the horizontal velocities. There are two possibilities, either no-slip or free-slip. For the former the tangential velocity u'_t vanishes on the boundary. For the latter the gradient of the tangential velocity at the boundaries must vanish. Requiring the gradient to vanish satisfies the free slip condition because it implies that the stress at the boundary (which is given by $\nu \partial u'_t/\partial z$) vanishes. In this case continuity implies that $d^2\hat{W}/dz^2 = 0$ that, when coupled with (51), yields the additional requirement, $d^4\hat{W}/dz^4 = 0$.

To investigate the stability of the free-slip system (which turns out to be the simplest to analyze) we look for non-vanishing real components of ω. It is straightforward to show that solutions of the form

$$\hat{W}(z) = \sum_{n=1}^{\infty} A_n \sin(n\pi z) \tag{59}$$

satisfy the boundary conditions for the free-slip boundary conditions. When substituted into (56) for the case of purely real growth rate, $(\omega = \omega_r)$, the following characteristic equation results:

$$\left(n^2\pi^2 + k^2\right)\left(n^2\pi^2 + k^2 + \omega\right)\left(n^2\pi^2 + k^2 + Pr\,\omega\right) = k^2\,Ra\,, \tag{60}$$

where it is left as an exercise to show that oscillatory solutions (those with $\omega_i \neq 0$) do not exist. For the case of marginal stability (*i.e.,* , $\omega_r = 0$), (60) yields a condition on the Rayleigh number as a function of the convective mode:

$$Ra = Ra_c = \frac{(n^2\pi^2 + k^2)^3}{k^2}. \tag{61}$$

The behavior of the critical Rayleigh number (Ra_c) as a function of n and k can be investigated. We note that $\partial Ra/\partial n > 0$ for $n > 0$ and that

$$\frac{\partial Ra_c}{\partial k} = 0 \quad \Longrightarrow \quad k^2 = \frac{(n\pi)^2}{2}. \tag{62}$$

Taken together these results imply that the most unstable mode is the $n = 1$ mode with $k^2 = k_c^2 = n^2\pi^2/2$. The value of the associated Rayleigh number is thus $Ra_c = 27\pi^4/4 \approx 658$. Physically this tells us how hard we have to force the flow before it convects. Before this limit we can imagine that the molecular transport of heat is sufficiently efficient to accomplish the heat transfer without macroscopic overturning.

The Rayleigh-Benard problem can be extended considerably. The marginal stability limit for varying boundary conditions (as shown in Table 1); the effect of a mean wind; the rotational effects; weakly non-linear transition regimes; and the pattern selection for the convection can all be explored. Scaling laws for the fully developed regime can also be investigated, of particular interest is the $Ra \to \infty$ limit. Apart from its analytic tractability the flow configuration also lends itself well to laboratory experiments. For these reasons Rayleigh-Benard convection is perhaps the most studied and most enduring paradigm for convection, although its applicability to the atmosphere is limited.